SCIENCE CHINA
Chemistry

•REVIEWS•
SPECIAL ISSUE: Celebrating the 100th Anniversary of Chemical Sciences in Nanjing University

May 2020 Vol.63 No.5: 619–636
https://doi.org/10.1007/s11426-020-9707-4

Chiral metal phosphonates: assembly, structures and functions

Guo-Guo Weng & Li-Min Zheng*

State Key Laboratory of Coordination Chemistry, School of Chemistry and Chemical Engineering, Collaborative Innovation Centre of Advanced Microstructures, Nanjing University, Nanjing 210023, China

Received January 2, 2020; accepted February 18, 2020; published online April 14, 2020

As an important class of inorganic-organic hybrid materials, metal phosphonates can exhibit versatile structures, interesting functions and high water and thermal stabilities. Despite a large number of metal phosphonates reported in the past two decades, the development of chiral metal phosphonates is still in its infancy. This review summarizes the current status in this topical field including the synthetic strategies, the crystal structures of chiral metal phosphonates reported thus far, and their physical and chemical properties. Future challenges in this promising field are also discussed.

chiral, metal, phosphonate, structure, property

Citation: Weng GG, Zheng LM. Chiral metal phosphonates: assembly, structures and functions. *Sci China Chem*, 2020, 63: 619–636, https://doi.org/10.1007/s11426-020-9707-4

1 Introduction

Chirality is a universal phenomenon in nature and life, which is closely related to the normal progress of biological processes [1]. Apart from its importance in pharmaceutical chemistry, chirality also plays a key role in material science. The controlled preparation of chiral functional structures is a highly demanded but challenging task for materials science because of the difficulties in synthesizing specific chiral assemblies with interesting properties [2]. Recently metal-organic hybrid materials have gained tremendous attention because they can exhibit precise structures and predictable functions that can be designed and constructed through judicious choice of metal ions and ligands. Among them, chiral metal-organic hybrid materials are of particular interest owing to their potential applications in enantioselective catalysis and separation, nonlinear optics, sensors, and other materials science [3–7].

Metal phosphonates are an important class of metal-organic hybrid materials that integrate organic and inorganic characteristics within a single molecular composite [8]. Compared with other metal-organic systems, metal phosphonates often show high water and thermal stabilities due to the presence of inorganic components such as clusters, chains or layers, which are essential for application purpose. The organic moieties of the phosphonate ligands RPO_3^{2-} can be modified by other functional groups resulting in new structure types and also bringing new functions. Recent progress in this field has been highlighted in a book [9] and several review articles [10–16]. However, despite the emergence of a number of new metal phosphonates in the past two decades, those with homochiral or enantioenriched characters are extremely limited in number. The main reason includes the limited chiral pool of the phosphonate ligands and the synthetic challenges in isolating crystalline chiral metal phosphonates. The first homochiral metal phosphonate was reported in 1999 by Bujoli and co-workers [17]. They employed an enantiopure ligand (*R*)-$H_2O_3PCH_2P(O)(CH_3)(C_6H_5)$ with a chiral P center and constructed a layered compound (*R*)-α-$Zn\{O_3PCH_2P(O)(CH_3)(C_6H_5)\}\cdot H_2O$. Two related chiral zinc phosphonates were also isolated afterwards [18]. Later Lin and co-workers [19–21] introduced

*Corresponding author (email: lmzheng@nju.edu.cn)

binaphthyl groups with axial chirality into metal phosphonate frameworks which show interesting asymmetric catalytic and chiral separation properties. Further development in this field has resulted in many new chiral metal phosphonates with variable structures and functions. Considering the biological importance of phosphorous compounds, it is interesting to observe for the first time the chiral transcription and amplification from molecular level to macroscopic level in a chiral lanthanide aminophosphonate system [22]. In this review, we wish to provide a comprehensive introduction of the current status in this field, including the synthetic strategies, crystal structures, morphology chirality, and the physical and chemical properties. According to the synthetic routes, the structures of the chiral metal phosphonates are described in the following sequence: (1) those obtained from achiral precursors, (2) obtained from chiral phosphonate ligands, and (3) obtained from chiral co-ligands. It should be mentioned that metal phosphonates crystallizing in chiral space groups but appearing as bulk racemic conglomerates are not included in this review. Finally, future challenges in this promising field are discussed.

2 Synthetic strategies

Like the other chiral metal-organic hybrid materials [23–25], chiral metal phosphonates can be constructed through the following three approaches: (1) the spontaneous symmetry breaking upon crystallization from achiral building blocks; (2) using enantiopure phosphonate ligands; (3) combining achiral phosphonate ligands with other chiral co-ligands.

The first approach seems to be economically appealing and desirable. However, this process occurs randomly and usually results in optically inactive conglomerates, e.g., a mechanical and racemic mixture of enantiomeric chiral crystals. Only in rare cases asymmetric chiral amplification of crystallization is achieved from achiral sources by symmetry breaking giving bulk products with enantiomeric excess. The symmetry breaking could be driven by supramolecular interactions such as hydrogen bond and π-π interactions. The enantiomer excess from achiral precursors could also be induced by chiral template, chiral solvent or chiral catalysis [25].

The second approach is more efficient and straightforward to obtain homochiral metal phosphonates. However, the syntheses of chiral phosphonate ligands are often tedious and expensive. This approach is largely limited by the chiral pool of the phosphonate ligands.

The third approach could provide a potentially large amount of chiral metal phosphonates considering that there are many other chiral ligands available such as natural amino acids. Unfortunately, very few examples of this type have been reported so far.

All the known chiral metal phosphonates have been assembled through these three approaches. Their crystal structures are described below.

3 Crystal structures

3.1 Chiral metal phosphonates using achiral phosphonate ligands

Although a number of metal phosphonates with versatile structures have been constructed using various asymmetric phosphonate ligands, few of them crystallize in chiral space groups through spontaneous resolution. The bulk products are frequently found to be optically inactive conglomerates. The asymmetric chiral amplification of crystallization from achiral sources by symmetry breaking remains to be a great challenge. Only in rare cases enantioenriched or even homochiral metal phosphonates were isolated starting from achiral ligands (Table 1), as described below.

A good example is provided by the achiral asymmetric ligand 2-carboxyphenylphosphonic acid (2-cppH$_3$,

Table 1 Enantioenriched metal phosphonates using achiral precursors

Compound	Space group	Structural features	Ref.
$(VO)_3$(2-cpp)$_2$$(H_2O)_6$•2$H_2O$ (**1**)	$P2_1$	2D double-layer containing corner-sharing {VO_6} or {VO_5} and {PO_3C}	[29]
[Cu(4-cppH)(2,2′-bipy)(H_2O)] (**2**)	$P2_1$	1D helical chain with {CuN_2O_3} cross-linked by 4-cppH ligands	[32]
Co_2(4-cnapp)$(OH)(H_2O)_2$ (**3**)	$P2_12_12_1$	3D framework with Δ-type chain of Co_3(μ_3-OH) linked by 4-cnapp ligands	[33]
Mn(2-pmamp)(H_2O) (**4**)	$P2_1$	2D layer with Mn(2-pmamp) connected by {PO_3C} via corner-sharing	[34]
[C_4mim][$(UO_2)_2$(1,3-pbpH)$_2$•(Hmim)] (**5**)	$P2_12_12_1$	3D framework with the inorganic chains cross-linked by 1,3-pbpH	[35]
Co(tbpH_2)(4,4′-bipy)•H_2O (**6**)	$P2_1$	3D framework with the inorganic chains cross-linked by tbpH_2 and 4,4′-bipy	[36]
Cs(*S*-HppaH_2) (**7**)	$P2_12_12_1$	3D framework with {CsO_x} polyhedral connected by {PO_3C}	[37]

Scheme 1). This ligand can offer three phosphonate oxygen and two carboxylate oxygen donors for coordination with metal ions. The chelation of the ligand to the octahedral metal ion can generate a chiral metal center. However, chiral transfer throughout the network structure is rather intriguing, and can be easily blocked when there exists a centrosymmetric center in the structure. This is indeed the case for layer compounds [M(2-cppH)(H_2O)] (M^{II}=Mn, Co, Ni) [26], M_3(2-cpp)$_2$(H_2O)$_3$•H_2O (M^{II}=Co, Zn) [27] and [H_3O]$_2$[Cu(H_2O)]$_2$[(UO_2)$_3$(2-cpp)$_4$]$_2$•3H_2O [28], where one of the three phosphonate oxygen atoms acts as μ_3-O bridging two metal ions leading to a centrosymmetric dimer of M_2O_2 within the structure. On the contrary, layer compound (VO)$_3$(2-cpp)$_2$(H_2O)$_6$•H_2O (**1**) [29] crystallizes in a chiral space group $P2_1$, unlike the other related M/2-cpp compounds which crystallize in centrosymmetric space groups. The phosphonate and carboxylate oxygen atoms are each coordinated to a single vanadium atom, thus chiral transfer is successfully achieved throughout the layer structure which is composed of corner-sharing {VO_5} square pyramids (or {VO_6} octahedra) and {PO_3C} tetrahedra (Figure 1). More interestingly, chiral symmetry breaking occurs upon crystallization with an enantiomeric excess of the bulk sample. Noting that the compound crystallizes in the form of clusters, different crystals from the same cluster also give different flack parameters, suggesting different level of enantiomeric excess. The origin of such an unusual symmetry breaking phenomenon could be attributed to the cooperation of the asymmetric ligand of 2-cpp^{3-}, the presence of multiple chiral centers (V, P) and the twisted layer structure. Partial release of the coordination water molecules upon heating leads to the transformation of {VO_6} octahedra into {VO_5} tetragonal pyramids and, therefore, the structure becomes centrosymmetric.

The 4-carboxyphenylphosphonic acid (4-cpppH_3) is a positional isomeric ligand of 2-cpppH_3. It reacts with metal ion forming a series of M/4-cpp compounds crystallizing in centrosymmetric space groups [30,31]. The lack of obvious chelating rings around the metal centers could be a reason for the formation of centrosymmetric structures. By incorporating 2,2′-bipy as co-ligand, Sun and co-workers [32] reported a copper compound [Cu(4-cppH)(2,2′-bipy)(H_2O)] (**2**) showing a chiral helical chain structure with space group $P2_1$. Within the structure, the Cu(II) ions are chelated by 2,2′-bipy and bridged by 4-cppH^{2-} ligands. Although its bulk sample appears as a conglomerate due to spontaneous resolution on crystallization, homochiral species can be obtained by utilizing the (+)-cinchonine or (−)-cinchonidine as a chiral-inducing agent.

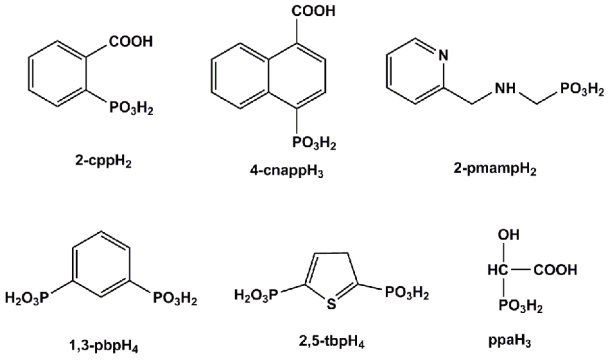

Scheme 1 Molecular structures of 2-cpppH_2, 4-cnapppH_3 and 2-pmamppH_2, 1,3-pbppH_4, 2,5-tbppH_4 and ppapH_3.

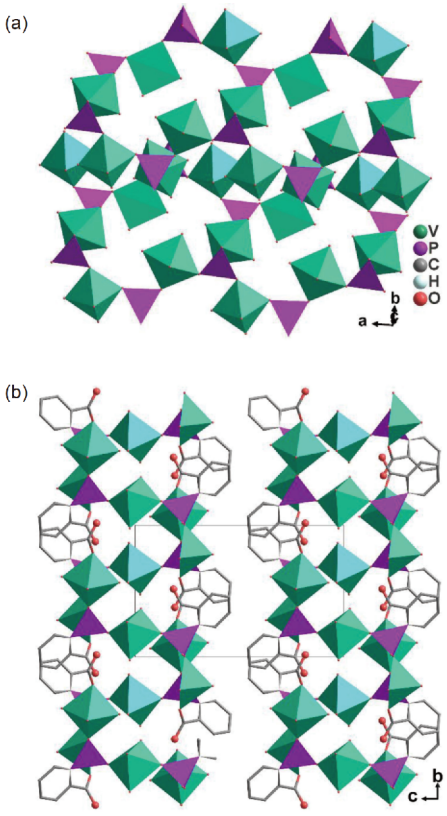

Figure 1 (a) The inorganic layer and (b) packing diagram of structure (VO)$_3$(2-cpp)$_2$(H_2O)$_6$•H_2O (**1**), adapted with permission from Ref. [29], copyright by Royal Society of Chemistry (2012) (color online).

The achiral (4-carboxynaphthalen-1-yl)phosphonic acid (4-cnapppH_3, Scheme 1) is analogues to 4-cpppH_3 except that the aromatic moiety is expanded in the former case. This could enhance the asymmetric nature of the ligand. By reacting 4-cnapppH_3 with cobalt salt, we isolated compound Co_2(4-cnapp)(OH)(H_2O)$_2$ (**3**) crystallizing in an orthorhombic space group $P2_12_12_1$ [33]. The bulk sample is again enantioenriched due to symmetry breaking on crystallization. This compound shows a three-dimensional framework structure in which the Δ-type chains of corner-sharing Co_3(μ_3-OH) triangles are cross-linked by the organic groups of the phosphonate ligands (Figure 2). Magnetic properties are studied.

The introduction of two chelating rings around the metal center in the framework structure could be an asset to the chirality maintenance and transmission. A good candidate of

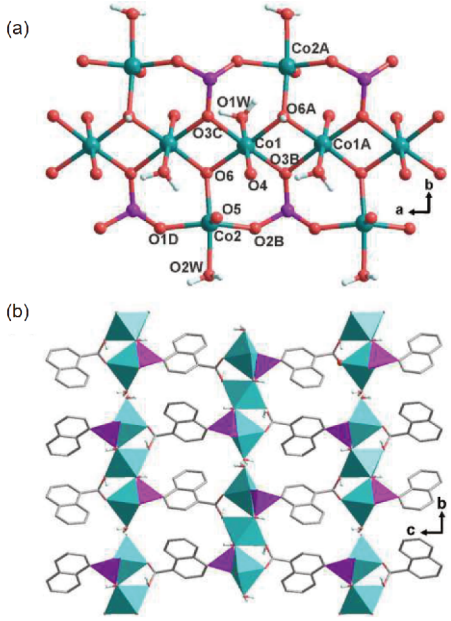

Figure 2 (a) Inorganic chain structure (b) packing diagram of compound Co_2(4-cnapp)(OH)(H_2O)$_2$ (**3**), adapted with permission from Ref. [33], copyright by American Chemical Society (2016) (color online).

such ligand is (2-pyridylmethylamino)methylphosphonate (2-pmampH_2, Scheme 1). It can provide two N and one phosphonate O atoms to form two five-membered chelating rings with metal ion generating chiral metal center, and another two phosphonate O atoms to connect the metal ions into a network structure. By reacting 2-pmampH_2 with metal salts under hydrothermal conditions, we obtained compounds M(2-pmamp)(H_2O) (M=Mn, Cd) crystallizing in chiral space groups $P2_1$ and $P2_12_12_1$, respectively [34]. Both compounds show similar layer structures in which neutral M(2-pmamp) units containing two five-membered rings are interlocked by two phosphonate O atoms (Figure 3). The only difference is the packing mode of the layers being AAAA in Mn(2-pmamp)(H_2O) (**4**) and ABAB in Cd(2-pmamp)(H_2O). The interlayer interactions are dominated by van der Waals forces. Apparently, chirality is successfully transferred from chiral metal centers to the layers and to the whole structure. Interestingly, although the bulk sample of the Cd compound appears as a racemic conglomerate, that of the Mn compound is enantioenriched as confirmed by solid-state CD spectra. Moreover, the bulk chirality is maintained after removal of the coordination water molecules. The dehydration process also induces a transformation of the magnetic properties, from antiferromagnetic to ferromagnetic.

Wang and co-workers [35] isolated a rare 3D chiral uranyl phosphonate via ionothermal reactions of uranyl nitrate and the achiral 1,3-phenylenebisphosphonic acid (1,3-pbpH_4, Scheme 1) in ionic liquid of 1-butyl-3-methylimidazoliumdibutylphosphate ([C_4mim][Dbp]). The resulted compound [C_4mim][(UO_2)$_2$(1,3-pbpH)$_2$·Hmim] (**5**) crystallizes in space group $P2_12_12_1$ with a Flack parameter of 0.193(10), indicating that the crystal was racemic conglomerate with one major enantiomer. The CD spectrum of bulk sample also suggested the excess of the major enantiomer. Within the structure, the {UO_6} and {PO_3C} polyhedra are connected through corner-sharing forming chains with 2_1 screw axis. The chains are further cross-linked by the phenyl groups of the 1,3-pbpH^{3-} ligands, leading to a 3D open framework with the channels filled by C_4mim^+ cations and protonated 1-methylimidazole (Figure 4). Interestingly similar reactions using different ionic liquids such as [C_4mpyr][Br] (*N*-butylmethylpyrrolidinium bromide) and [Etpy][Br] (*N*-ethylpyridinium bromide) resulted in compounds crystallizing in centrosymmetric space groups, indicating that the ionic liquid could play an important role in inducing the chirality of the uranyl phosphonates.

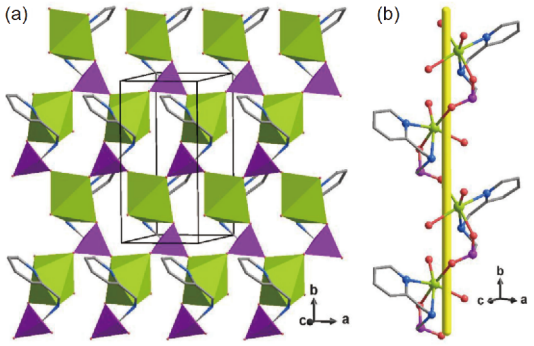

Figure 3 (a) One layer structure of Mn(2-pmamp)(H_2O) (**4**) viewed along the *c* axis; (b) right-handed helical chain running along the *b*-axis, adapted with permission from Ref. [34], copyright by American Chemical Society (2008) (color online).

2,5-Thiophene-bisphosphonic acid (2,5-tbpH_4, Scheme 1) is similar to 1,3-pbpH_4 except that the benzene ring in the latter is replaced by the thiophene group. Sun and co-workers

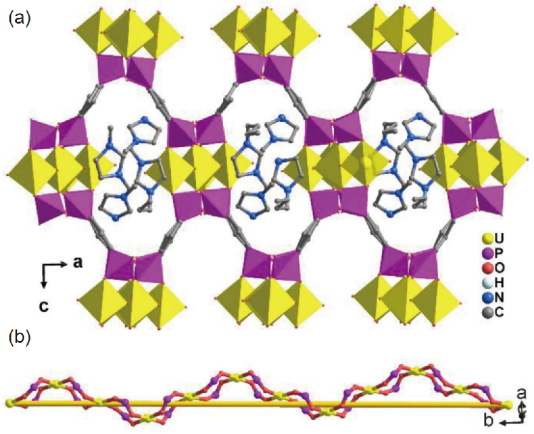

Figure 4 (a) Packing diagram of [C_4mim][(UO_2)$_2$(1,3-pbpH)$_2$•Hmim] (**5**). (b) A chiral chain of UO_6 units and PO_3C tetrahedra along the *b*-axis, adapted with permission from Ref. [35], copyright by Royal Society of Chemistry (2015) (color online).

[36] reported a 3D chiral cobalt(II) complex by combining achiral 2,5-tbpH$_4$ with 4,4′-bipy, namely, Co(2,5-tbpH$_2$)(4,4′-bipy)•H$_2$O (**6**). It crystallizes in monoclinic space group $P2_1$. Each Co atom is five-coordinated with a distorted trigonal-bipyramidal geometry, three equatorial positions occupied by the phosphonate oxygen atoms and two axial positions by bipyridine nitrogen atoms. The equivalent Co atoms are interconnected by 2,5-tbpH$_2^{2-}$ ligands via corner-sharing of {CoO$_3$N$_2$} and {PO$_3$C} polyhedra forming infinite helical chains. The chains are further linked by 4,4′-bipy into a 3D framework structure (Figure 5). Considering that the 2,5-tbpH$_4$ ligand is rigid and symmetric, the coordination with Co^{II} ions causes a slight conformation twist of the ligand which is believed to induce the symmetry breaking phenomenon. Interestingly the bulk sample of this compound is also enantioenriched, confirmed by both single crystal structural analyses and CD measurements.

Racemic ligands are another source of asymmetric ligands. The reactions of racemic phosphonic acids with metal salts usually result in the formation of racemic compounds or conglomerates. The only exception, as far as we are aware, is Cs(*S*-ppaH$_2$) (**7**) [37], where ppaH$_3$ represents 2-hydroxyphosphonoacetic acid (Scheme 1). This compound was obtained by reacting a racemic mixture of (*R*), (*S*)-ppaH$_3$ with CsCl in aqueous solution at room temperature. It crystallizes in the monoclinic space group $P2_12_12_1$. A 3D framework structure is found to contain only the *S*-isomer of the ligand. Within the structure, each ppaH^{2-} binds to five Cs$^+$ ions through chelating and bridging modes and each Cs$^+$ also connects to five equivalent ppaH^{2-} ligands. The bulk sample is enantioenriched, confirmed by ECD in solution exhibiting a negative dichroic signal at 210 nm. Notably, spontaneous resolution does not occur when Cs$^+$ is replaced by Li$^+$, Na$^+$ and K$^+$, suggesting that the spontaneous resolution upon crystallization could be size-dependent.

3.2 Chiral metal phosphonates using chiral phosphonate ligands

A direct and efficient method to obtain chiral metal phosphonates is using chiral phosphonate ligands as precursors. The chirality of organic ligands is usually generated in three ways: central chirality, axial chirality and facial chirality. The first concerns with single atom chirality originating from tetrahedral atoms such as carbon, silicon, sulfur, phosphorus and others. While in the latter two cases, no asymmetric atoms are present in the molecule [38]. So far the known chiral metal phosphonates contain ligands with central or axial chirality (Table 2). Those with facial chirality have not been reported. As this approach usually result in enantiopure bulk products confirmed by CD or VCD spectra, the bulk chirality is not discussed in this section except in the cases that racemization occurs.

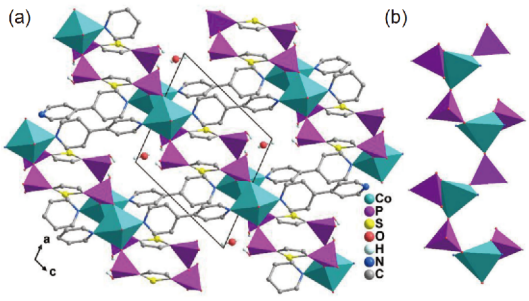

Figure 5 Packing diagram (a) and inorganic chain (b) of structure Co(2,5-tbpH$_2$)(4,4′-bipy)•H$_2$O (**6**), adapted with permission from Ref. [36], copyright by American Chemical Society (2016)(color online).

3.2.1 *Phosphonate ligands with central chirality*

(1) Phosphorous centered chiral phosphonate ligands. Compound (*R*)-α-Zn{O$_3$PCH$_2$P(O)(CH$_3$)(C$_6$H$_5$)}•H$_2$O (**8**) was the first enantiopure metal phosphonate reported by Bujoli *et al.* [17], where the ligand (*R*)-H$_2$O$_3$PCH$_2$P(O)(CH$_3$)(C$_6$H$_5$) has a chiral P center and both the phosphonate oxygen and phosphine oxide atoms are involved in the coordination with zinc atoms. It has a layer structure constructed by corner-sharing of alternating {ZnO$_4$} and {PO$_3$C} tetrahedra. The lattice water molecules reside between the layers. Replacement of the methyl by ethyl group results in a closely related compound (*R*)-α-Zn{O$_3$PCH$_2$P(O)(C$_2$H$_5$)(C$_6$H$_5$)}•H$_2$O (**9**) which possesses an identical layer topology (Figure 6(a)) but crystallizes in different space group (triclinic *P*1 for **9** vs. orthorhombic $P2_12_12_1$ for **8**). Notably, a new chiral phase formulated as (*R*)-β-Zn{O$_3$PCH$_2$P(O)(CH$_3$)(C$_6$H$_5$)}•H$_2$O (**10**) was isolated when the pH of the reaction mixture was lowered to 4.0 [18]. Although it also exhibits a layered structure, the phosphine oxide is not bonded to Zn (Figure 6(b)). Each Zn atom is octahedrally coordinated by four phosphonate oxygen atoms and two water molecules. Consequently, the layer is composed of infinite chains of edge-sharing {ZnO$_6$} octahedra and {PO$_3$C} linkages, completely different from that of the α-phase.

(2) Amino acid-derived chiral phosphonate ligands. The most commonly used chiral molecules possess chiral carbon centers, among which chiral amino acids and their derivatives are promising candidates. (*S*)-proline and its derivatives are good homogeneous catalysts in asymmetric synthesis. Therefore (*S*)-proline derived phosphonate ligands, especially (*S*)-1-phosphonomethylproline (H$_2$O$_3$PCH$_2$-NHC$_4$H$_7$-COOH, H$_3$L[1]) (Scheme 2), have been employed as chiral precursors in the syntheses of enantiopure metal phosphonates.

Qiu and co-workers [39] prepared a homochiral 3D zinc phosphonate (*S*)-Zn$_2$(O$_3$PCH$_2$NHC$_4$H$_7$CO$_2$)$_2$ (**11**) (Figure 7). It crystallizes in the orthorhombic space group $P2_12_12$, and shows a 3D open framework structure consisting of 4,8-nets

Table 2 Chiral metal phosphonates obtained using enantiopure phosphonate ligands or co-ligands

Compound	Space group	Structural features	Ref.
(*R*)-α-Zn{$O_3PCH_2P(O)(CH_3)(C_6H_5)$}•$H_2O$ (*R*-**8**)	$P2_12_12_1$	2D layer containing corner-sharing {ZnO_4} and {PO_3C}	[17]
(*R*)-α-Zn{$O_3PCH_2P(O)(C_2H_5)(C_6H_5)$}•$H_2O$ (*R*-**9**)	$P1$	2D layer containing corner-sharing {ZnO_4} and {PO_3C}	[18]
(*R*)-α-Zn{$O_3PCH_2P(O)(CH_3)(C_6H_5)$}•$H_2O$ (*R*-**10**)	$C2$	2D layer containing edge-sharing {ZnO_6} and {PO_3C} linkage	[18]
(*S*)-Zn_2{$O_3PCH_2NHC_4H_7CO_2$}$_2$ (*S*-**11**)	$P2_12_12$	3D framework containing 4,8-nets	[39]
(*S*)-[$Co_2Cl(HL^1)(H_2O)_5$]Cl•H_2O (*S*-**12**)	$P2_12_12_1$	3D framework with inorganic chains cross-linked by carboxylate groups	[42]
(*S*)-Sr_2(S-HL^1)$(NO_3)_2(H_2O)$•H_2O (*S*-**13**)	$P2_12_12_1$	2D layer with edge-sharing {SrO_x} chains linked by {PO_3C}	[42]
$Cd_2L^1Cl(H_2O)$ (**14**)	$P2_1$	2D layer with chains of edge-sharing Cd-octahedra linked by {PO_3C}	[43]
[$Zn_7L^1{}_6$][$Zn(H_2O)_6$]$_2$•$16H_2O$ (**15**)	$P2_13$	[$Zn_7L^1{}_6$] clusters packed to create micropore	[43]
[$Zn_9(L^2)_6(H_2O)_3$]•C_2H_5OH•$8.5H_2O$ (**16**)	$P1$	2D layer containing $Zn_7(L)_6$ clusters and {ZnO_4} linkages	[44]
[$Tb(H_2L^1)_3$]•$2H_2O$ (**17**)	$P4_1$	1D chain with {TbO_6} triply bridged by {PO_3C}	[45]
[$Dy(H_2L^1)_3$]•$2H_2O$ (**18**)	$P4_1$	1D chain with {DyO_6} triply bridged by {PO_3C}	[45]
[$Eu(H_2L^1)_3$]•$2H_2O$ (**19**)	$P4_1$	1D chain with {EuO_6} triply bridged by {PO_3C}	[45]
[$Gd(H_2L^1)_3$]•$2H_2O$ (**20**)	$P4_1$	1D chain with {GdO_6} triply bridged by {PO_3C}	[45]
(*S*)-$Co_3(ppap)_2$(4,4′-bpy)$_2(H_2O)_2$•$4H_2O$ (*S*-**21**)	$P2_1$	3D framework with inorganic chains linked by 4,4′-bpy	[46]
(*S*)-$Co_3(ppap)_2$(4,4′-bpy)$_2(H_2O)_2$•$3H_2O$ (*S*-**22**)	$P1$	2D layer with inorganic chains linked by 4,4′-bpy	[46]
[Ca(D-pmpcH)$(H_2O)_2$]•$2HO_{0.5}$ (**23**)	$P2_12_12_1$	2D layer with inorganic chains linked by *D*-pmpcH ligand	[47]
Cu(D-pmpcH)(CH_3OH) (**24**)	$P2_12_12_1$	1D chain with{CuO_4N} connected by carboxylate groups	[48]
Cu(D-pmpcH) (**25**)	$P2_12_12_1$	2D sheet with (4, 4) topology	[48]
Cd_2(D-pmpcH)$(H_2O)_2Cl_2$ (**26**)	$P2_12_12_1$	3D framework with cross-linked inorganic chains	[48]
(*R*)-, (*S*)-α-[Zn_2(pemp)(pempH)Cl] (**27**)	$P2_12_12_1$	2D layer containing corner-sharing {ZnO_3N} or {ZnO_3Cl} and {PO_3C}	[49]
(*R*)-, (*S*)-β-[Zn_2(pemp)(pempH)Cl] (**28**)	$P2_1$	2D layer containing corner-sharing {ZnO_3N} or {ZnO_3Cl} and {PO_3C}	[49]
(*S*)-[$Zn_4$$(pempH)_4(bdc)_2$]•$2H_2O$ (*S*-**29**)	$P2_12_12$	2D layer, inorganic double chains connected by bdc^{2-}	[50]
(*R*)-, (*S*)-[$Zn_3(pempH)_2(btc)(H_2O)_2$]•$H_2O$ (**30**)	$C2$	3D framework with inorganic chains linked by btc^{4-}	[50]
(*R*)-, (*S*)-Co(pemp)$(H_2O)_2$ (**31**)	$P6_3$	1D nanotube containing corner-sharing {CoO_5N} and {PO_3C}	[51].
(*R*)-, (*S*)-Ni(pemp)$(H_2O)_2$ (**32**)	$P6_3$	1D nanotube containing corner-sharing {NiO_5N} and {PO_3C}	[51]
(*R*)-, (*S*)-Fe(pemp)$(H_2O)_2$ (**33**)	$P6_3$	1D nanotube containing corner-sharing {FeO_5N} and {PO_3C}	[52]
(*R*)-, (*S*)-Mg(pemp)$(H_2O)_2$ (**34**)	$P6_3$	1D nanotube containing corner-sharing {MgO_5N} and {PO_3C}	[53]
(*R*)-[Mg_{10}(pemp)$_{10}(H_2O)_{10}$]•$3H_2O$ (*R*-**35**)	$P2_1$	2D layer containing squashed tubes	[53]
(*S*)-Eu(pempH)$(NO_3)_2(H_2O)_2$ (*S*-**36**)	$P2_1$	2D brick-wall-shaped layer of corner-sharing {EuO_9} and {PO_3C}	[54]
(*S*)-Tb(pempH)$(NO_3)_2(H_2O)_2$ (*S*-**37**)	$P2_1$	2D brick-wall-shaped layer of corner-sharing {TbO_9} and {PO_3C}	[54]
(*S*)-Ho(pempH)$(NO_3)_2(H_2O)_2$ (*S*-**38**)	$P2_1$	2D brick-wall-shaped layer of corner-sharing {HoO_9} and {PO_3C}	[54]
(*R*)-(H_3O)[$Tb_3(pempH_2)_2(pempH)_7$] [$Tb_3(pempH_2)(pempH)_8$]$(NO_3)_4$•$11H_2O$ (*R*-**39**)	$P2_1$	1D chain with Tb triply bridged by μ_3-O(P) and O–P–O units	[22]
(*R*)-, (*S*)-Tb$(pempH)_3$•$2H_2O$ (**40**)	$P6_5$, $P6_1$	1D chain with Tb triply bridged by two μ_3-O(P) and one O–P–O unit	[22]
(*R*)-$Tb_3(pempH_2)_2(pempH)_7(NO_3)_2$•$2H_2O$ (*R*-**41**)	$P2_12_12_1$	1D chain with Tb triply bridged by μ_3-O(P) and O–P–O unit	[22]
(*R*)-[$Dy_3(pempH)_7(pempH_2)_2$]$_2(NO_3)_4$•$12H_2O$ (*R*-**42**)	$P2_1$	1D chain with Dy triply bridged by μ_3-O(P) and O–P–O unit	[55]
(*R*)-, (*S*)-[$Dy_3(pempH)_7(pempH_2)_2$]Cl_2•$2H_2O$ (**43**)	$P2_12_12_1$	1D chain with Dy triply bridged by μ_3-O(P) and O–P–O unit	[55]
(*R*)-, (*S*)-[$Dy_3(pempH)_7(pempH_2)_2$]Br_2•$2H_2O$ (**44**)	$P2_12_12_1$	1D chain with Dy triply bridged by μ_3-O(P) and O–P–O unit	[55]
(*R*)-[$Dy_{11}(pempH_2)_6(pempH)_{27}$]$(CF_3SO_3)_6$•$22H_2O$ (*R*-**45**)	$P2_1$	1D chain with Dy triply bridged by μ_3-O(P) and O–P–O units	[55]
(*R*)-, (*S*)-[$Er_4(pempH)_{12}$]•$7H_2O$ (**46**)	$P6_5$, $P6_1$	1D chain containing triple-stranded helices	[56]
(*R*)-, (*S*)-[$Er_3(pempH)_7(pempH_2)_2$]$(NO_3)_2$•$2H_2O$ (**47**)	$P2_12_12_1$	1D chain containing triple-stranded helices	[56]

(*To be continued on the next page*)

(*Continued*)

Compound	Space group	Structural features	Ref.
(*R*)-, (*S*)-[Er_2(pempH)$_4$(NO_3)Cl] (**48**)	$P2_12_12$	1D chain containing quadruple-stranded helices	[56]
(*R*)-[Er_2(pempH)$_4Cl_2$] (*R*-**49**)	$P2_12_12$	1D chain containing quadruple-stranded helices	[56]
(*R*)-, (*S*)-(Me_3Sn)$_2$(pemp)(H_2O) (**50**)	$P2_1$	1D chain with Me_3Sn bridged by O-P-O	[57]
(*R*)-, (*S*)-(Ph_3Sn)$_2$(pemp)$_2$ (**51**)	$P2_12_12_1$	1D chain with Ph_3Sn bridged by O-P-O	[57]
(*S*)-Co_2(μ_3-OH)(cyamp)(CH_3COO) (*S*-**52**)	$P2_1$	2D layer with Δ-type chains of Co_3(μ_3-OH) linked by {PO_3C}	[58]
(*S*)-Co_2(μ_3-OH)(cyamp)($C_7H_{15}COO$) (*S*-**53**)	$P2_1$	2D layer with Δ-type chains of Co_3(μ_3-OH) linked by {PO_3C}	[58]
(*R*)-Gd(H_2L^3)(H_3L^3)(H_2O)$_4$•*x*H_2O (*R*-**59**)	$P2_12_12_1$	2D grid with Gd atoms connected by H_2L^3 and H_3L^3 ligands	[19]
(*R*)-Ni(H_2L^3)(MeOH)$_4$ (*R*-**61**)	$P2_12_12_1$	1D chain with Ni atoms connected H_2L^3 ligands	[20]
(*R*)-Zn_3(HL^3)$_2$(py)$_2$ (*R*-**62**)	$C2$	2D layer with inorganic chains connected by HL^3 ligands	[20]
(*R*)-Mn(H_2L^3)(MeOH)•MeOH (*R*-**63**),	$P2_12_12_1$	3D framework with inorganic chain cross-linked by H_2L^3 ligands	[20]
(*R*)-Co_2(H_2L^3)$_2$(H_2O)$_3$•4H_2O (*R*-**64**)	$P2_1$	3D framework with inorganic chain cross-linked by H_2L^3 ligands	[20]
(*R*)-Cu(L^3-Et_2) (*R*-**65**)	$P2_12_12_1$	3D framework with inorganic chain cross-linked by L^3-Et ligands	[20]
(*R*)-[Nd_2(HL^4)$_2$($MeOH$)$_8$]•H_4L^4•3HCl•6H_2O (*R*-**66**)	$C2$	2D layer with inorganic chains linked by HL^4 ligands	[21]
(*R*,*R*)-, (*S*,*S*)-Mn(5-Brsalcy)(2-$FC_6H_4PO_3H$)]•3H_2O (**68**)	$P2_1$	1D chain with [Mn^{III}(5-Brsalcy)]$^+$ bridged by O-P-O units	[59]
(*R*,*R*)-[Mn(5-Brsalcy)(4-$CH_3C_6H_4PO_3H$)]•CH_3OH•H_2O (**69**)	$P2_1$	1D chain with [Mn^{III}(5-Brsalcy)]$^+$ bridged by O-P-O units	[59]

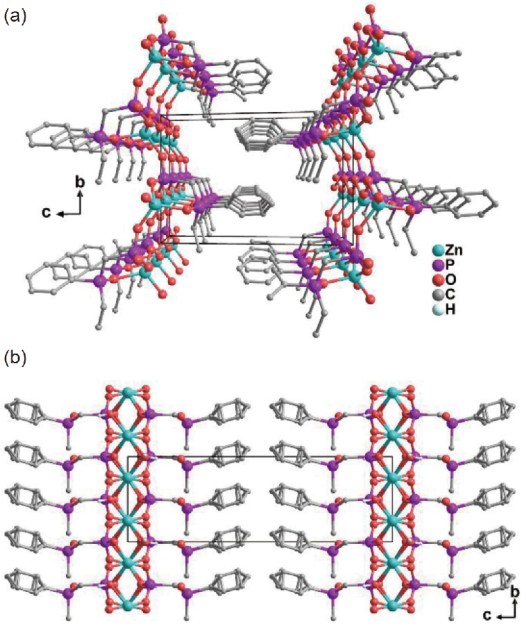

Figure 6 Packing diagrams of structures **9** (a) and **10** (b), adapted with permission from Ref. [18], copyright by Royal Society of Chemistry (2001) (color online).

formed by alternately arranged left- and right-handed helices that are connected via the phosphonate ligands. Two crystallographically distinguished {ZnO_4} and {PO_3C} tetrahedra are observed. Each {ZnO_4} shares three vertex oxygen atoms with {PO_3C} and *vice versa* forming inorganic layer. Neighboring layers are connected by the organic groups of H_2L^1 ligands forming an open framework. The framework contains two types of helical channels with dimensions 4×6 and 5×12 Å viewed along the *c*-axis. The amino group and the partially uncoordinated carboxylate group, which are the active sites for asymmetric catalysis, are retained and directed into the channels. Unfortunately, however, the catalytic properties were not investigated.

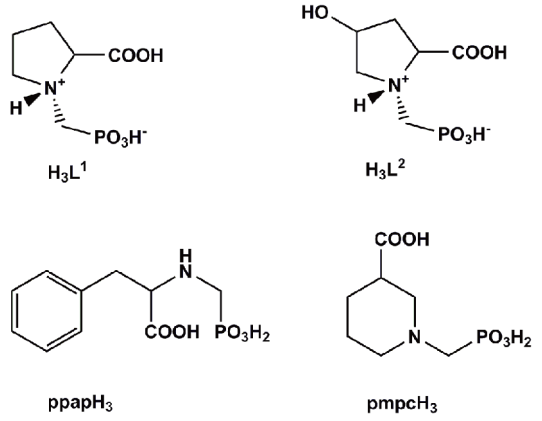

Scheme 2 Molecular structures of H_3L^1, H_3L^2, $ppapH_3$ and $pmpcH_3$.

Notably, the formation of homochiral metal phosphonates using chiral amino acid-derived phosphonic acids is not always guaranteed. Hix and co-workers [40] prepared compound $Co_3(O_3PCH_2\text{-}NHC_4H_7\text{-}COO)_2$•5$H_2O$ by hydrothermal treatment of a mixture of (*S*)-H_3L^1 and $Co(OAc)_2$ at 160 °C. This compound crystallizes in a centrosymmetric space group *P*−1. Pairs of edge-sharing {CoO_6} octahedra are connected through corner-sharing forming chains, and the chains are further connected by the {PO_3C} tetrahedra via corner-sharing into a layer structure. Another example is $Pb_4O(O_3PCH_2\text{-}NHC_4H_7\text{-}COO)_2$ obtained by hydrothermal

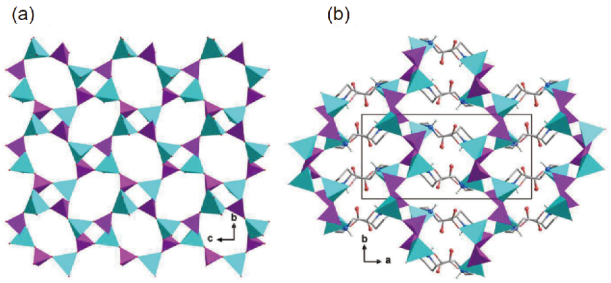

Figure 7 (a) Single inorganic layer and (b) packing diagram of structure (*S*)-$Zn_2\{O_3PCH_2NHC_4H_7CO_2\}_2$ (**11**). All H atoms are omitted for clarity. Cyan: $\{ZnO_4\}$, purple: $\{PO_3C\}$, red: O, grey: C, adapted with permission from Ref. [39], copyright by John Wiley & Sons, Inc. (2004)(color online).

reaction at 180 °C, which is non-chiral and crystallizes in space group P_{-1} [41].

The reason for the racemization of amino acid is not clear and could be related to high temperature of hydrothermal reaction. By reacting the same phosphonic acid with $CoCl_2$ under mild condition, Mao and co-workers [42] isolated compound $Co_2Cl(S\text{-}HL^1)(H_2O)_5]Cl\bullet H_2O$ (**12**) from aqueous solution at room temperature. This compound crystallizes in a chiral space group $P2_12_12_1$, and shows a homochiral 3D framework structure. Edge-sharing dimers of $\{CoO_5Cl\}$ are linked by the $\{PO_3C\}$ into left-handed helical chains running along the *a*-axis. The equivalent chains are further cross-linked by the (*S*)-H_3L^1 ligands through the coordination of the carboxylate groups, forming a 3D framework with helical channels running long the *a*- and *b*-axes. Similar reaction with $Sr(NO_3)_2$ resulted in a layer compound $Sr_2(S\text{-}HL^1)(NO_3)_2(H_2O)\bullet H_2O$ (**13**) crystallizing in the same space group. In this case, chains of edge-sharing $\{Sr1O_8\}$ and $\{Sr2O_9\}$ are connected alternatively by the phosphonate groups forming a layer. The proline groups are pendant on the two sides of the layer. Unfortunately the yields of both products are extremely low, thus detailed characterization of the materials was not possible.

It is worth mentioning that high temperature could not be the only reason for racemization of the amino acid. Mao and co-workers [43] synthesized another three compounds under hydrothermal conditions at 170 or 160 °C. Compounds $Cd_2L^1Cl(H_2O)$ (**14**) with a layer structure and $[Zn_7L^1{}_6][Zn(H_2O)_6]_2\bullet 16H_2O$ (**15**) with a framework structure crystallize in chiral space groups $P2_1$ and $P2_13$, respectively, whereas compound $[Pb_2Cl_2(HL^1)]$ with a layer structure crystallizes in a centrosymmetric space group $P2_1/c$.

Racemization of (*S*)-1-phosphonomethylproline was also found by Cheng and co-workers [44] in synthesizing compound $[Zn_9(L^1)_6(H_2O)_2]\bullet 13.5H_2O$ through hydrothermal reactions at 160 °C. The compound is racemic crystallizing in space group *P*31*c*. It has a layer structure containing clusters of $Zn_7(L^1)_6$ interconnected by the $\{ZnO_4\}$ tetrahedra through carboxylate groups of the ligand. To maintain the chirality of the ligand, they proposed to introduce a second chiral center. 1-Phosphonomethyl-4-hydroxyproline (H_4L^2, Scheme 2) was thus synthesized, based on which compound $[Zn_9(L^2)_6(H_2O)_3]\bullet C_2H_5OH\bullet 8.5H_2O$ (**16**) was obtained under similar reaction conditions. Indeed this compound crystallizes in the triclinic chiral space group *P*1 even though the –OH group is not involved in the coordination with metal ions. Similar Zn_7 cluster building units are found which are connected by the $\{ZnO_4\}$ and $\{ZnO_5\}$ polyhedra through carboxylate oxygen atoms into a chiral layer structure (Figure 8). Apparently introducing multiple chiral sites into the phosphonate ligands could be a good way to avoid the racemization of the chiral ligand even at high reaction temperature. Luminescent properties were also studied.

When an excess amount of (*S*)-H_3L^1 was allowed to react with $LnCl_3$ under hydrothermal conditions at 100 °C, chain compounds $[Ln(H_2L^1)_3]\bullet 2H_2O$ [Ln=Tb (**17**), Dy (**18**), Eu (**19**), Gd (**20**)] were isolated by Chen and co-workers [45]. They are isostructural crystallizing in the tetragonal chiral space group $P4_1$ (Figure 9). The Ln^{III} has severely distorted octahedral geometry with the six coordination sites occupied by six H_2L^1 anions. The equivalent Ln^{III} ions are triply bridged by O-P-O units forming a triple-strand helical chain running along the *c*-axis. Neighboring chains are stacked through hydrogen bonds to form a 3D supramolecular framework which can host the right-handed helical chains of water. The adsorption and luminescent properties were investigated.

Another amino-acid derivative is (*R*)-, (*S*)-3-phenyl-2-[(phosphonomethyl)amino]propanoic acid ($ppapH_3$, Scheme 2). We isolated two pairs of enantiopure compounds (*R*)-, (*S*)-$Co_3(ppap)_2(4,4'\text{-}bpy)_2(H_2O)_2\bullet 4H_2O$ (**21**) and (*R*)-, (*S*)-

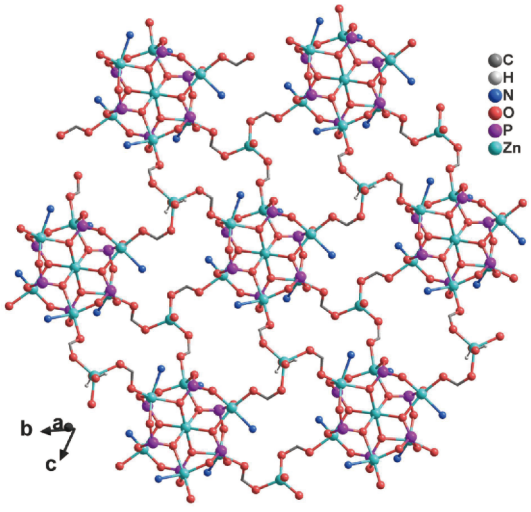

Figure 8 The layer structure of $[Zn_9(L^2)_6(H_2O)_3]\bullet C_2H_5OH\bullet 8.5H_2O$ (**16**). All C atoms except the carboxylate groups, H atoms except those in water molecules and the lattice solvents are omitted for clarity, adapted with permission from Ref. [44], copyright by Wiley-VCH Verlag GmbH (2009) (color online).

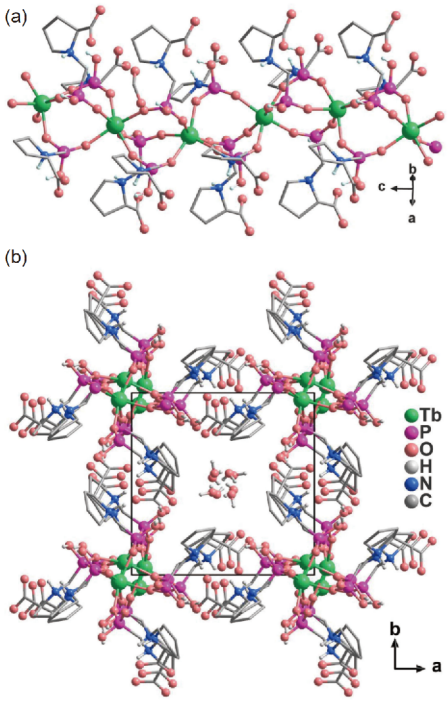

Figure 9 (a) Helical chain in structure $[Tb(H_2L^1)_3]\cdot 2H_2O$ (**17**) running along the crystallographic 4_1 axis; (b) packing diagram of structure **17** viewed along the *c*-axis, adapted with permission from Ref. [45], copyright by American Chemical Society (2006) (color online).

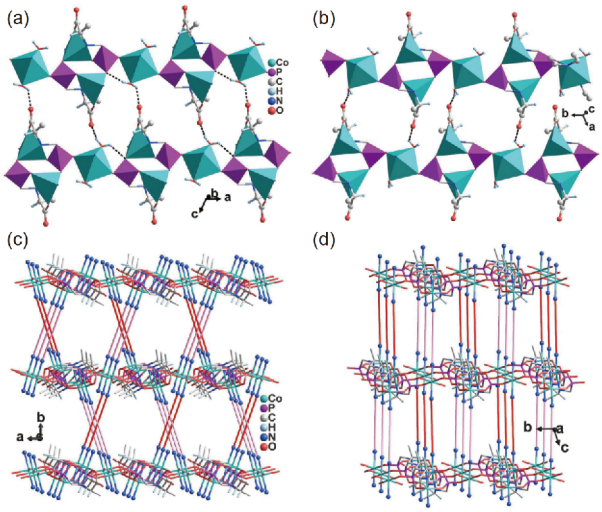

Figure 10 (a, c) Supramolecular layers made up of hydrogen-bonded cobalt phosphonate chains and (b, d) packing diagrams for (*S*)-**21** (a, b) and (*S*)-**22** (c, d). The red and pink lines represent crystallographically different 4,4′-bpy molecules. Hydrogen bonds are indicated by dotted black lines. The lattice water molecules and phenyl rings are omitted for clarity, adapted with permission from Ref. [46], copyright by Wiley VCH (2015) (color online).

$Co_3(ppap)_2(4,4'\text{-bpy})_2(H_2O)_2\cdot 3H_2O$ (**22**) crystallizing in chiral space groups $P2_1$ and $P1$, respectively [46]. Compounds **21** and **22** are catenation isomers, formation of which is controlled solely by the pH of the reaction mixture. They contain similar inorganic chiral chains made up of $\{CoO_3N_2\}$, $\{CoO_4N_2\}$ and $\{PO_3C\}$ polyhedra with slightly different bond lengths and angles (Figure 10(a, c)). The chains are connected by moderate strong hydrogen bonds into a supramolecular layer and also by 4,4′-bipyridine (4,4′-bpy) by coordination bonds (Figure 10(b, d)). Significantly, each chain in **21** is linked to four other equivalents *via* 4,4′-bpy forming a 3D framework, whereas each chain in **22** is connected to two other equivalent chains through 4,4′-bpy forming 2D layer. When racemic $ppapH_3$ is used, achiral *Rac*-$Co_3(ppap)_2(4,4'\text{-bpy})_2(H_2O)_2\cdot 4H_2O$ was obtained, which possesses the same molecular composition and identical 3D framework structure with that of **21** but crystallizes in centrosymmetric space group $P2_1/c$. Therefore the formation of isomeric compounds **21** and *Rac*-$Co_3(ppap)_2(4,4'\text{-bpy})_2(H_2O)_2\cdot 4H_2O$ is controlled by the chirality of the phosphonate ligands.

1-(Phosphonomethyl)piperidine-3-carboxylic acid ($pmpcH_3$, Scheme 2) can be viewed as a derivative of β-amino acid. Based on D-$pmpcH_3$, Zhu and co-workers [47,48] synthesized several homochiral compounds including $[Ca(D\text{-}pmpcH)(H_2O)_2]\cdot 2HO_{0.5}$ (**23**), Cu(D-pmpcH)(CH_3OH) (**24**), Cu(D-pmpcH) (**25**) and Cd_2(D-pmpcH)$(H_2O)_2Cl_2$ (**26**). All crystallize in space group $P2_12_12_1$. Compound **24** shows a 1D helical chain structure in which the $\{CuO_4N\}$ square pyramids are connected by carboxylate groups. The phosphonate groups reside on the two sides of the chain. Compounds **23** and **25** show 2D layer structures. In **23**, the Ca centers are connected by chelating and bridging phosphonate oxygen atoms into a chain, and the neighboring chains are further connected by the organic groups of the ligands. While in **25**, chains of corner-sharing $\{CuO_4N\}$ and $\{PO_3C\}$ are connected by the carboxylate groups into a layer (Figure 11(a, b)). Compound **26** shows a 3D diamondoid architecture. Within the structure, dimers of edge-sharing $\{CdO_4Cl_2\}$ are found, which are linked by $\{PO_3C\}$ through corner-sharing into a chain (Figure 11(c)). Each chain is connected to its four equivalents via corner-sharing of $\{CdO_4Cl_2\}$, thus forming a chiral 3D framework (Figure 11 (d)). Proton conductive properties were studied.

(3) Chiral amino-phosphonate ligands. The optically active amino phosphonic acids can be viewed as mimics of natural amino acids, by using phosphonic acid to replace carboxylic acid group. Based on (*R*)-, (*S*)-(1-phenylethylamino)methylphosphonic acid ($pempH_2$, Scheme 3), we and others have obtained a series of homochiral metal phosphonates with versatile structures.

(*R*)- and (*S*)-α-$[Zn_2(pemp)(pempH)Cl]$ (**27**) are enantiomers crystallizing in space group $P2_12_12_1$ (Figure 12) [49]. They exhibit layer structures made up of alternatively corner-sharing $\{ZnO_3N\}$ (or $\{ZnO_3Cl\}$) and $\{PO_3C\}$ tetrahedra. Interestingly, similar reactions in the presence of organic molecules or at a higher reaction temperature lead to

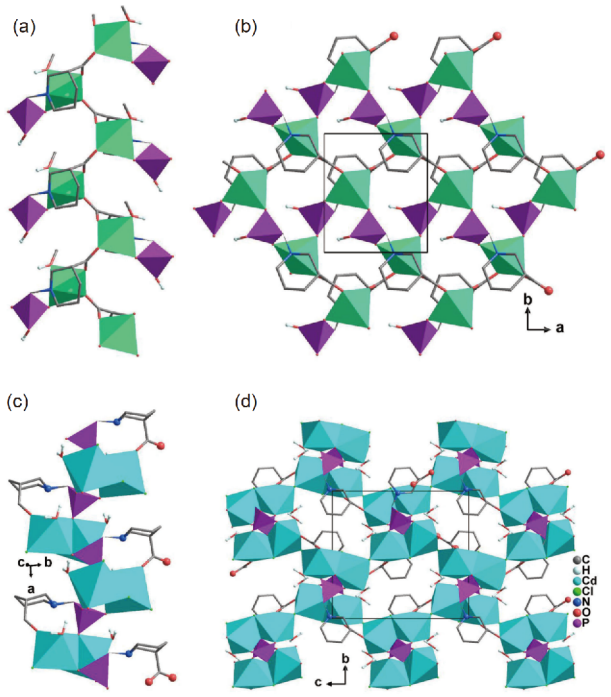

Figure 11 (a) The carboxylate bridged chain and (b) layer structure of Cu(D-pmpcH) (**25**). (c) The phosphonate bridged chain and (d) 3D framework structure of Cd_2(D-pmpcH)$(H_2O)_2Cl_2$ (**26**), adapted with permission from Ref. [48], copyright by Royal Society of Chemistry (2017) (color online).

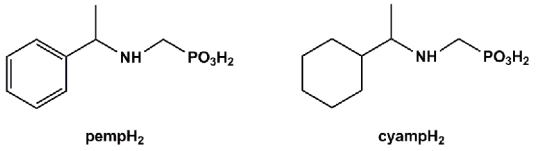

Scheme 3 Molecular structures of $pempH_2$ and $cyampH_2$.

the formation of polymorphic phases of (*R*)-, (*S*)-β-[Zn_2(pemp)(pempH)Cl] (**28**) that crystallize in space group $P2_1$. The main difference between the α- and β-phases is the packing mode of layers which is ABAB in the α-phase and AAAA in the β-phase. The incorporation of 1,4-benzenedicarboxylic acid (H_2bdc) or 1,2,4,5-benzenetetracarboxylic acid (H_4btc) as second linkers results in homochiral compounds (*R*)-, (*S*)-[Zn_4(pempH)$_4$(bdc)$_2$]•2H_2O (**29**) or (*R*)-, (*S*)-[Zn_3(pempH)$_2$(btc)$(H_2O)_2$]•H_2O (**30**) [50]. Compounds **29** show 2D layer structures in which double-chains made up of corner-sharing {ZnO_4} and {PO_3C} tetrahedra are connected by bdc ligand. In compounds **30**, the corner-sharing tetrahedra of {ZnO_4} and {PO_3C} are linked to form a zigzag chain containing four-membered rings, which are further linked by μ_4-btc forming a 3D chiral open framework. The generated chiral channels are filled with organic residues of $pempH^-$ and lattice water.

Noting that the phosphonate ligands in compounds **29** and **30** were not fully deprotonated, the pH of the reaction mixture was increased and isostructural compounds (*R*)-, (*S*)-M^{II}

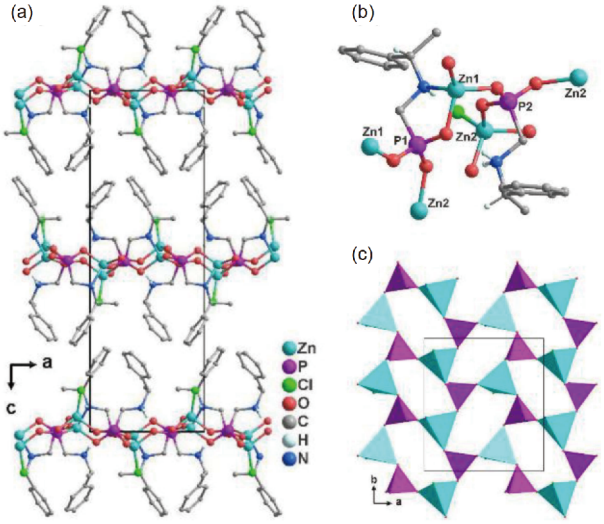

Figure 12 (a) Packing diagram of (*R*)-α-[Zn_2(pemp)(pempH)Cl] (*R*-**27**) along the *b* axis. (b) Coordination geometries of Zn atoms in **27**. (c) Inorganic layer of structure *R*-**27**, adapted with permission from Ref. [49], copyright by American Chemical Society (2008) (color online).

(pemp)$(H_2O)_2$ [M=Co (**31**), Ni (**32**), Fe (**33**), Mg (**34**)] with nanotubular structures were obtained successfully under hydrothermal conditions [51–53]. In these compounds, all three phosphonate oxygen donors and the amino N atom are involved in the coordination with metal ions forming purely inorganic tube wall containing corner-sharing {MO_5N} octahedra and {PO_3C} tetrahedra (Figure 13). The coordination of the amino group could pose a chemical pressure and facilitate the formation of a tubular instead of a layer structure.

Although homochirality remains after removal of the coordination water, the dehydrated sample can only adsorb small molecules such as water due to their narrow channel. Interestingly, compound *R*-**33** shows highly selective nitric oxide adsorption properties, attributed to the presence of unsaturated and redox-active iron sites [52]. A systematic study on the Mg/$pempH_2$ system reveals that compounds **34**

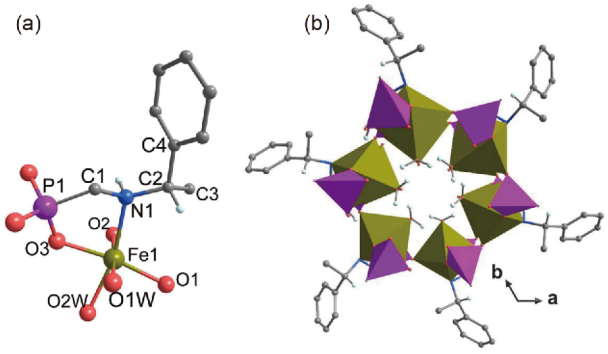

Figure 13 (a) The building unit of structure *R*-Fe(pemp)$(H_2O)_2$ (*R*-**33**); (b) the single nanotube viewed along the *c*-axis. All H atoms except those attached to N, water O and chiral C atoms are omitted for clarity, adapted with permission from Ref. [52], copyright by Royal Society of Chemistry (2019) (color online).

can transform into (*R*)-, (*S*)-[$Mg_{10}(pemp)_{10}(H_2O)_{10}$]•$3H_2O$ (**35**) in a reversible manner by adjusting the temperature and pH (Figure 14). The structures of **35** can be described as 2D layers containing squashed tubes [53].

The reactions of $pempH_2$ and $Ln(NO_3)_3$ in aqueous solution at room temperature result in homochiral isostructural compounds $Ln(pempH)(NO_3)_2(H_2O)_2$ [Ln=Eu (**36**), Tb (**37**), Ho (**38**)] [54]. They show brick-wall-shaped layer structures containing 2_1 helical chains, where each {EuO_9} polyhedron is corner-shared with three {PO_3C} tetrahedra and *vice versa*. The Eu and Tb compounds display characteristic red and green luminescent properties (Figure 15).

By conducting the reactions under hydrothermal conditions with increased molar ratio of $pempH_2$ and $Tb(NO_3)_3$, we obtained block-like crystals of (*R*)-, (*S*)-(H_3O)[$Tb_3(pempH_2)_2(pempH)_7$][$Tb_3(pempH_2)(pempH)_8$]$(NO_3)_4$•$11H_2O$ (**39**) at pH 2.8–3.0 and rod-like crystals of (*R*)-, (*S*)-$Tb(pempH)_3$•$2H_2O$ (**40**) at pH 3.7–4.5, respectively [22]. Compounds **39** crystallize in chiral space group $P2_1$, and contain two types of positively charged chains, e.g., chain I with composition $[Tb_3(pempH_2)_2(pempH)_7]^{2+}$ and chain II with composition $[Tb_3(pempH_2)(pempH)_8]^{+}$ in which the Tb^{III} ions are triply bridged by two μ_3-O(P) and one O-P-O forming left-handed triple-stranded helical chains. While **40** crystallize in chiral space group $P6_5$ or $P6_1$. A neutral chain structure is found (chain III), where the adjacent Tb atoms are triply bridged by one μ_3-O(P) and two O-P-O units into a left-handed triple-stranded helical chain along the *c*-axis. Studies on the *R*-isomers reveal that *R*-**39** undergoes a solid state structural transformation soon after exposure to air at room temperature, forming (*R*)-$Tb_3(pempH_2)_2(pempH)_7(NO_3)_2$•$2H_2O$ (*R*-**41**) which crystallizes in space group $P2_12_12_1$ (Figure 16).

Noting that the positively charged chains in **39** are balanced by negatively charged anion which reside between the

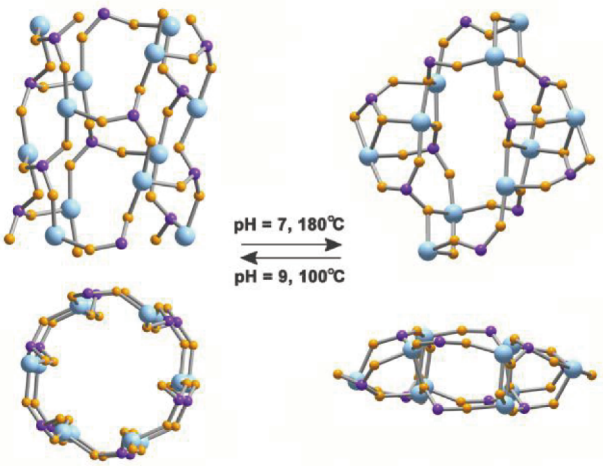

Figure 14 Interconversion of structures (*R*)-$Mg(pemp)(H_2O)_2$ (**34**) (left) and (*R*)-$[Mg_{10}(pemp)_{10}(H_2O)_{10}]$•$3H_2O$ (**35**) (right), adapted with permission from Ref. [53], copyright by Wiley VCH (2017) (color online).

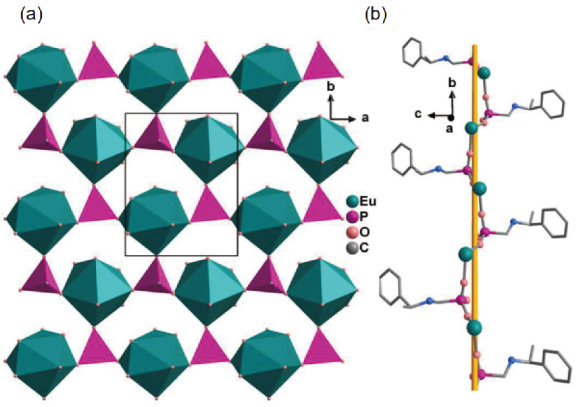

Figure 15 (a) The brick-wall-shaped inorganic layer of ***S*-36**. (b) A helical chain within the layer running along the *b* axis, adapted with permission from Ref. [54], copyright by American Chemical Society (2009) (color online).

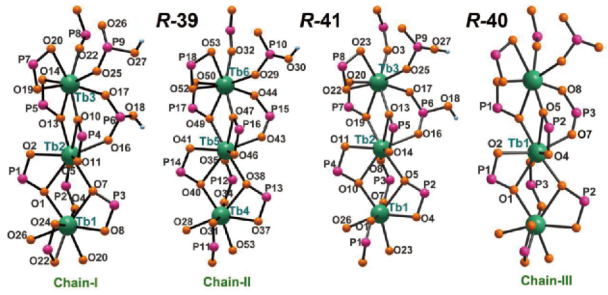

Figure 16 Chain structures with atomic labelling in *R*-**39**, *R*-**41** and *R*-**40** along the crystallographic 2_1 or 6_5 screw axis. The N and C atoms are omitted for clarity, adapted with permission from Ref. [22], copyright by Springer Nature (2017) (color online).

chains, we envisage that the crystal morphology (or aspect ratio) and the properties of similar chain compounds could be modulated by the counter-anions. The dysprosium ion was chosen to construct chain compounds analogues to **39** because of previous success in producing high performance single molecule magnets (SMM). By using different dysprosium salts DyX_3 ($X=NO_3^-$, Cl^-, Br^-, $CF_3SO_3^-$), we obtained four pairs of enantiopure compounds (*R*)-, (*S*)-[$Dy_3(pempH)_7(pempH_2)_2]_2(NO_3)_4$•$12H_2O$ (**42**), (*R*)-, (*S*)-[$Dy_3(pempH)_7(pempH_2)_2$]X_2•$2H_2O$ [X=Cl (**43**), Br (**44**)] and (*R*)-, (*S*)-[$Dy_{11}(pempH_2)_6(pempH)_{27}$]$(CF_3SO_3)_6$•$22H_2O$ (**45**) [55]. The morphology study on the *R*-isomers reveals that the aspect ratio follows the sequence: *R*-**42** (NO_3^-)<*R*-**43** (Cl^-)<*R*-**44** (Br^-)<*R*-**45** ($CF_3SO_3^-$), in agreement with the decreasing interchain interactions involving counter-anions. The result is supported by molecular simulations. The counter-anions also show prominent influences on the intrachain structures and the local coordination geometries of the Dy^{III} ions and thus their magnetic behavior.

Another interesting observation is the salt-assisted conversion of helical structures from triple-stranded to quadruple-stranded helices based on homochiral Er^{III}-$pempH_2$

systems. By reacting $Er(NO_3)_3$ with (*R*)-, (*S*)-pempH$_2$ at different pH under hydrothermal conditions, we obtained two pairs of enantiopure compounds (*R*)-, (*S*)-[Er_4(pempH)$_{12}$]•7H_2O (**46**) and (*R*)-, (*S*)-[Er_3(pempH)$_7$(pempH$_2$)$_2$]$(NO_3)_2$•2H_2O (**47**) with chain structures [56]. Structure *R*-**46** contains two kinds of chains with compositions Er(pempH)$_3$ and Er_3(pempH)$_9$, respectively. The Er atoms are triply bridged by one μ_3-O(P) and two O-P-O units in the former, and by two μ_3-O(P) and one O-P-O units in the latter. Compound *R*-**47** contains cationic chains and NO_3^- anions in the structure, and is isostructural to the Tb and Dy analogues. Remarkably, salt-assisted structural transformation occurs after adding a suitable amount of NaCl to the reaction mixture of *R*-**46**, first to *R*-**47** and then to (*R*)-[Er_2(pempH)$_4(NO_3)$Cl] (*R*-**48**). A complete conversion from *R*-**47** to *R*-**48** is also observed upon NaCl addition (Figure 17). Compounds **48** exhibit quadruple-stranded helical chain structures in which the Er atoms are connected by pairs of O-P-O units along the *c*- and *b*-axes. The direct reaction of $ErCl_3$ and (*R*)-, (*S*)-pempH$_2$ in the presence of NaCl results in compound (*R*)-, (*S*)-[Er_2(pempH)$_4Cl_2$] (**49**) which has similar structures to those of **48**. The conversion from triple-stranded to quadruple-stranded helical structures simply by adding salts was not reported before for the coordination polymer systems, which could be related to the significant change of the ionic strength in the reaction mixture. Luminescent properties were also investigated.

By using the same pempH$_2$ ligands, Ma and co-workers [57] reported two pairs of organotin phosphonates (*R*)-, (*S*)-$(Me_3Sn)_2$(pemp)(H_2O) (**50**) and (*R*)-, (*S*)-$(Ph_3Sn)_2$(pemp)$_2$ (**51**). All possess homochiral chain structures. In **50** each phosphonate ligand binds to three Me_3Sn using its three oxygen donors, as shown in Figure 18. While in **51** each phosphonate ligand binds to two Ph_3Sn using two of its three oxygen donors. Weak hydrogen bond interactions are present between the chains. Cytostatic activity against HeLa or HepG-2 cell lines was also studied.

[(1-Cyclohexylethyl)amino]methylphosphonic acid (cyampH$_2$, Scheme 3) is analogous to pempH$_2$ except that cyclohexyl replaces the phenyl group. However, the only examples reported so far are enantiopure isomers of (*R*)-, (*S*)-$Co_2(\mu_3$-OH)(cyamp)(C_nH_{2n+1}COO) [*n*=1 (**52**), 7 (**53**)] (Figure 19) [58]. They crystallize in chiral space group $P2_1$, and show layer structures. The inorganic layers are composed of Δ-type chains of corner-sharing triangles of $Co_3(\mu_3$-OH), interconnected by the O-P-O groups. The interlayer spaces are filled with the organic residues of the phosphonate and carboxylate ligands which determine the interlayer distances and hence their magnetic properties.

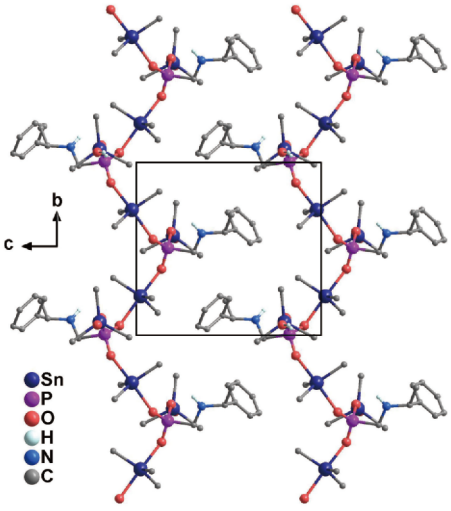

Figure 18 Packing diagram of structure (*R*)-$(Me_3Sn)_2$(pemp)(H_2O) (*R*-**50**), adapted with permission from Ref. [57], copyright by Elsevier (2019) (color online).

3.2.2 *Phosphonate ligands with axial chirality*

The binaphthylene derivatives are typical axially chiral ligands due to the hindered rotation of the C–C single bond that connects the two aryl groups. Although they have been widely used in constructing porous materials for chiral separation and asymmetric catalysis, few compounds have been reported containing binaphthalene-phosphonate li-

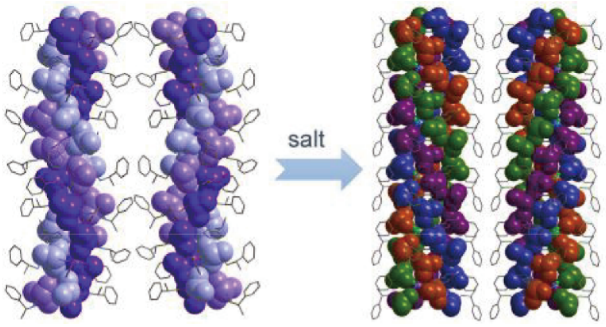

Figure 17 Structural conversion from *R*-**47** and *S*-**47** to *R*-**48** and *S*-**48**, respectively, in the presence of NaCl, adapted with permission from Ref. [56], copyright by American Chemical Society (2018) (color online).

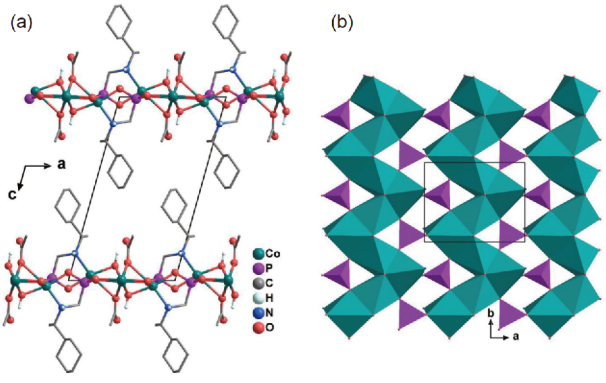

Figure 19 (a) The packing diagram and (b) inorganic layer of structure (*S*)-$Co_2(\mu_3$-OH)(cyamp)(CH_3COO) (**52**), adapted with permission from Ref. [58], copyright by Wiley VCH (2014) (color online).

gands. Lin and co-workers synthesized a series of compounds based on 2,2′-diethoxy-1,1′-binaphthylene-6,6′-bisphosphonic acid (H_4L^3) and 2,2′-pentaethyleneglycol-1,1′-binaphthyl-6,6′-bisphosphonic acid (H_4L^4), as shown in Scheme 4.

Compounds (*R*)-, (*S*)-Ln(H_2L^3)(H_3L^3)$(H_2O)_4$•xH_2O [Ln=La (**54**), Ce (**55**), Pr (**56**), Nd (**57**), Sm (**58**), Gd (**59**), Tb (**60**); x=9–14] were obtained by slow evaporation of an acidic mixture of nitrate or perchlorate salts of lanthanide and H_4L^3 in methanol at room temperature [19]. They are isostructural, confirmed by the PXRD measurements. Single crystal structural analysis on *R*-**59** reveals that it crystallizes in space group $P2_12_12_1$ and has a 2D rhombohedral grid-like layer structure in which the Gd centers are connected by the partially protonated H_2L^3 and H_3L^3 ligands (Figure 20). The binaphthyl subunits have dihedral angles of 118.2° and 121.0° for H_2L^3 and H_3L^3, respectively. The layers are packed along the *b*-axis, forming a 3D supramolecular network containing channels with the largest dimension of ca. 12 Å.

The reactions of the same phosphonic acid with transition metal salts under solvothermal conditions result in pairs of enantiopure compounds (*R*)-, (*S*)-Ni(H_2L^3)$(MeOH)_4$ (**61**), (*R*)-, (*S*)-$Zn_3(HL^3)_2(py)_2$ (**62**), (*R*)-, (*S*)-Mn(H_2L^3)(MeOH)•MeOH (**63**), (*R*)-, (*S*)-$Co_2(H_2L^3)_2(H_2O)_3$•$4H_2O$ (**64**) and (*R*)-, (*S*)-Cu(L^3-Et_2) (**65**) [20]. Single crystal structural analyses were performed for the *R*-isomers. **61** has a chain structure in which H_2L^3 serves as a bidentate ligand connecting the Ni^{II} ions into a zigzag chain. **62** exhibits a 2D layer structure where inorganic chains made up of corner-sharing $\{ZnO_4\}$ and $\{PO_3C\}$ are connected by the organic groups of HL^3. Each HL^3 acts as a penta-dentate ligands binding to five Zn atoms. Compounds **63**–**65** show 3D framework structures, where inorganic chains of corner-sharing $\{MO_x\}$ (x=4–6) and $\{PO_3C\}$ are cross-linked by the organic groups of the phosphonate ligands. The inorganic chains in **63** and **65** are quite similar in which the five-coordinated Mn^{II} or four-coordinated Cu^{II} ions are doubly bridged by O-P-O units into chains. While in **64**, the six-coordinated Co^{II} ions are bridged by single and double O-P-O units alternatively into a chain (Figure 21). The channel sizes are 5.3 Å×2.7 Å for **63** and 3.4 Å×4 Å for **64**. For **65**, the channel is filled by ethyl groups of ligand and thus no guest molecule can reside within the channel. The luminescent properties of **62** and **63** are investigated.

By taking the advantage of robust framework of metal phosphonates and enantioselectivity of chiral crown ethers, Lin *et al.* [21] designed the ligand H_4L^4 and synthesized compounds (*R*)-, (*S*)-$[Ln_2(HL^4)_2(MeOH)_8]$•H_4L^4•3HCl•$6H_2O$ [Ln=Nd (**66**), Sm (**67**)]. **66** and **67** are isostructural. Single crystal structural determination on *R*-**66** reveals that it crystallizes in chiral space group *C*2. Two Nd atoms are crystallographically distinguished, each adopts a square antiprismatic geometry. The Nd1 and Nd2 are doubly bridged by O-P-O units alternatively forming a chain. Adjacent chains are connected by binaphthyl backbones leading to a 2D lamellar structure (Figure 22). The chiral crown ether groups are placed between the layers. Interestingly, however, the lamellae are intercalated with free H_4L^4 molecules which result in smaller porosity and preclude its application in bulk chiral separations.

3.3 Chiral metal phosphonates using chiral co-ligands

Another efficient but much less explored approach toward

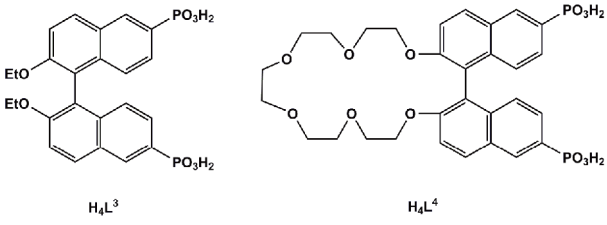

Scheme 4 Molecular structures of binaphthalene-6,6′-bisphosphonic acids.

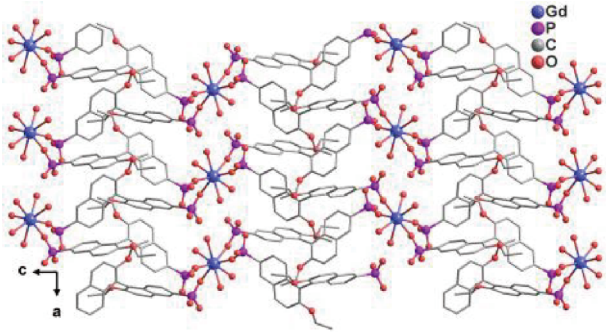

Figure 20 One layer of structure *R*-Gd(H_2L^3)(H_3L^3)$(H_2O)_4$•xH_2O (*R*-**59**), adapted with permission from Ref. [19], copyright by American Chemical Society (2001) (color online).

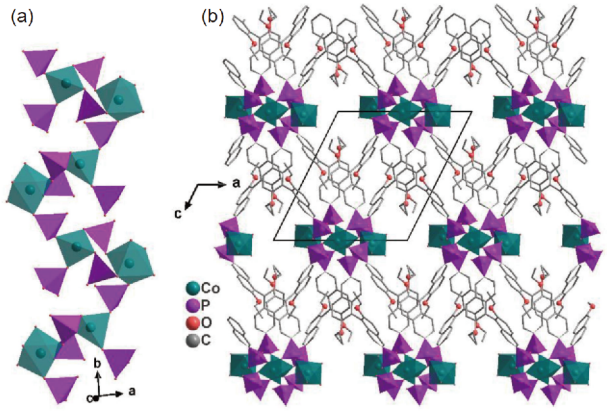

Figure 21 (a) The inorganic chain and (b) packing diagram of structure *R*-$Co_2(H_2L^3)_2(H_2O)_3$•$4H_2O$ (**64**), adapted with permission from Ref. [20], copyright by American Chemical Society (2002) (color online).

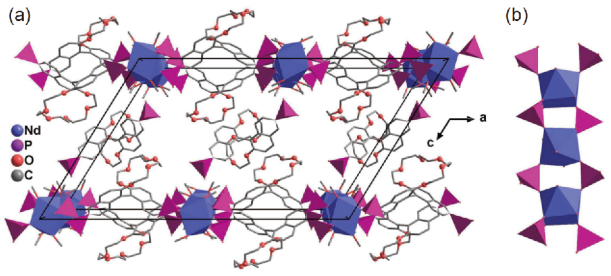

Figure 22 (a) The packing diagram and (b) inorganic chain of structure *R*-[$Nd_2(HL^4)_2(MeOH)_8$]•H_4L^4•3HCl•6H_2O (**66**), adapted with permission from Ref. [21], copyright by American Chemical Society (2002) (color online).

chiral metal phosphonates is using chiral co-ligands. Chiral Mn^{III} Schiff-base complexes have been well developed as asymmetric catalysts. By combining (*R*,*R*)- or (*S*,*S*)-Mn(5-Brsalcy)$^+$ [5-Brsacy=*N*,*N*′-(1,2-cyclohexane diylethylene)-bis(5-bromosalicylideneiminato)] with achiral 2-FPhPO_3H_2 or 4-CH_3PhPO_3H_2, we obtained two couples of enantiomers, namely, (*R*,*R*)-, (*S*,*S*)-Mn(5-Brsalcy) (2-$FC_6H_4PO_3H$)]•3H_2O (**68**), and (*R*,*R*)-, (*S*,*S*)-[Mn(5-Brsalcy)(4-$CH_3C_6H_4PO_3H$)]•CH_3OH•H_2O (**69**) [59]. In all cases, chiral monomeric species of [Mn^{III}(5-Brsalcy)]$^+$ are bridged purely by O-P-O units of different phosphonate ligands forming infinite chains (Figure 23). Second-order nonlinear effect was observed. The magnetic properties were also studied.

4 Chiral expression of metal phosphonates from molecular to macroscopic level

Biological chirality is not only limited to molecular chirality caused by chiral central atom but also includes structural chirality in the topological geometric space. For example,

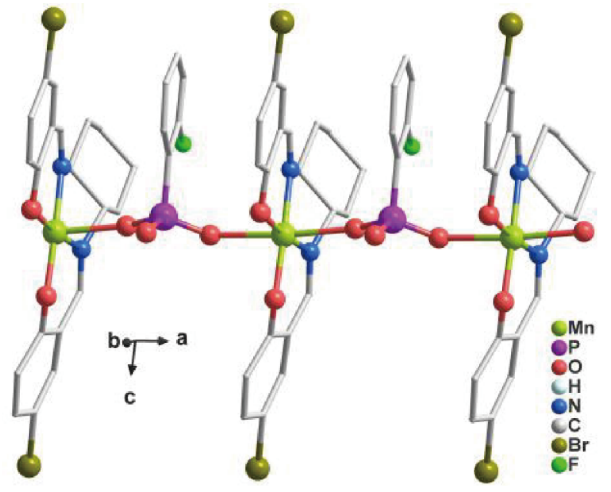

Figure 23 Chain structure of compound (*S*,*S*)-Mn(5-Brsalcy) (2-$FC_6H_4PO_3H$)]•3H_2O (**68**), adapted with permission from Ref. [59], copyright by Royal Society of Chemistry (2013) (color online).

condensation of L-amino acids leads to the formation of chiral peptides, which further assemble into helical proteins through weak intermolecular interactions. It remains a challenging task, however, to achieve chirality transcription and amplification from molecular level to helical structure in synthetic systems. Considering that weak interactions such as π-π stacking, hydrogen bonding and hydrophobic interactions are important in assembling biomolecules with hierarchical structures, the selection of suitable organic ligands and the control of weak interactions between the chain or layer motifs could be a key for the construction of homochiral coordination polymers in crystalline and helical morphologies.

By using optically active amino phosphonic acid pempH$_2$, we succeeded in assembling the first homochiral metal phosphonates with helical morphologies [22]. As already described in Sect. 3.2.1-(3), the reactions of pempH$_2$ and $Tb(NO_3)_3$ resulted in block-like crystals of (*R*)-, (*S*)-(H_3O)-[Tb_3(pempH$_2$)$_2$(pempH)$_7$][Tb_3(pempH$_2$)(pempH)$_8$](NO_3)$_4$•11H_2O (**39**) at pH 2.8–3.0 and rod-like crystals of (*R*)-, (*S*)-Tb(pempH)$_3$•2H_2O (**40**) at pH 3.7–4.5, respectively. The former contains positively charged chains of [Tb_3(pempH$_2$)$_2$-(pempH)$_7$]$^{2+}$ and [Tb_3(pempH$_2$)(pempH)$_8$]$^+$, while the latter contains neutral chains of Tb(pempH)$_3$. Interestingly, homochiral helices of (*R*)-, (*S*)-Tb(pempH)$_3$•2H_2O (**70**) can be obtained when the pH of the reaction mixture is kept in between (ca. 3.1). Helices **70** are identical to crystalline compounds **40** not only in the chemical composition but also in the PXRD patterns except that the peaks are all left-shifted to lower angles. Obviously, the helices of **70** have a high degree of crystallinity with almost the same structure at the molecular level as that of rod-like crystals of **40**, but at macroscopic level different from **40**.

Based on both the experimental and simulation results, we proposed the formation mechanism of the helices of **70** as illustrated in Figure 24. When there exists pure positively charged chains at lower pH (2.8–3.0) or pure neutral chains at higher pH (3.7–4.5), crystalline block-like (**39**) or rod-like materials (**40**) would be obtained. When pH is in between (ca. 3.1), both neutral and positively charged chains coexist in the same reaction solution. The binding of the positively charged chains to the neutral ones triggers the twist of chain growth. The twisted chains further assemble into hierarchical bundles, finally forming **70** with a 1D helical morphology. Both pH and the nitrate anion play vital roles in the formation of the helices.

5 Properties and applications

Chiral materials have been widely studied for potential applications in enantioselective catalysis and separation, nonlinear optics, chiral sensing and other material science.

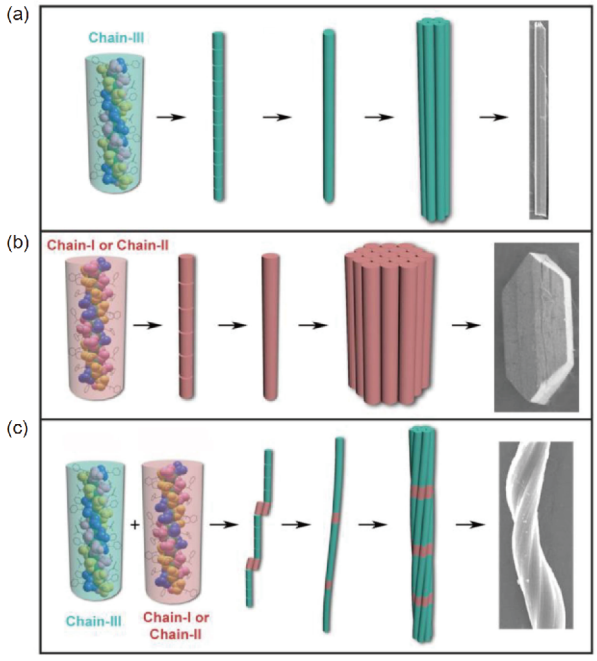

Figure 24 Proposed formation mechanism of helices. Formation mechanisms of crystalline materials of *R*-**40** (a) and *R*-**39** (b), and helices of *R*-**70** (c), adapted with permission from Ref. [22], copyright by Springer Nature (2017) (color online).

However, the main focus of chiral metal phosphonates so far has been on the syntheses and structural descriptions. Only in limited cases, the asymmetric catalytic properties and other functions have been explored, as discussed below.

5.1 Asymmetric catalysis and chiral separation

Lin and co-workers [19] synthesized compounds (*R*)-, (*S*)-Ln(H_2L^3)(H_3L^3)$(H_2O)_4$•xH_2O [Ln=La (**54**), Ce (**55**), Pr (**56**), Nd (**57**), Sm (**58**), Gd (**59**), Tb (**60**); x=9–14] with good stability and reversibility of the dehydration process. The presence of both Lewis and Brönsted acid sites in **54**–**60** rendered them capable of catalyzing several organic transformations including cyanosilylation of aldehydes and ring opening of *meso*-carboxylic anhydrides. The cyanosilylation reactions using different aldehydes afforded good yields (⩾55%) but the products were essentially racemic (ee<5%). Similar results were found for the ring opening reactions of *meso*-anhydrides. Enantioselective separation of racemic *trans*-1,2-diamonocyclohexane was also tried with ammonia-treated (*R*)-**58** which gave an enantio-enrichment of 13.6% in (*S*,*S*)-1,2-diamonocyclohexane in the beginning fractions and an enantio-enrichment of 10.0% in (*R*,*R*)-1,2-diamonocyclohexane in the ending fractions.

We tested the catalytic properties of homochiral compound (*S*)-[Tb(pempH)$(NO_3)_2(H_2O)_2$] (**37**) [54]. The dehydrated sample showed catalytic activities related to the Biginelli reaction in a yield of 50% and, again, the products were essentially racemic (ee<5%).

To increase the enantio-selectivity, Lin *et al.* designed and synthesized a series of chiral porous zirconium phosphonates in which the enantiopure and catalytically active Ru species are involved (Scheme 5). Compounds with approximate formulae [Zr{Ru(L^5)$(DMF)_2Cl_2$}]•2MeOH (**71**) and [Zr{Ru-(L^6)$(DMF)_2Cl_2$}]•2MeOH (**72**) [60] were found to be highly active catalysts for asymmetric hydrogenation of β-keto esters. **71** catalyzed the hydrogenation of a wide range of β-alkyl-substituted β-keto esters with complete conversions and ee values up to 95.0% and can be readily recycled and reused. While **72** catalyzed the same reactions with modest ee values. The enantioselective hydrogenation of unfunctionalized aromatic ketones was also studied using related chiral Zr[Ru(L^5)$(DPEN)Cl_2$]•$4H_2O$ (**73**) and Zr[Ru-(L^6)$(DPEN)Cl_2$]•$4H_2O$ (**74**) as catalysts [61]. The result demonstrated that **73** catalyzed heterogeneous asymmetric hydrogenation of aromatic ketones with practically useful, remarkably high activity and enantioselectivity up to 99.2% ee. Similarly, the asymmetric Mukaiyama Aldol reaction of 1-methoxy-2-methyl-1-trimethylsiloxy-1-propene and benzaldehyde was tested using a layered Zr compound containing *N*-(*m*-solfophenyl)-L(+)-valine-phosphonate ligand as catalyst [62]. A porous, homochiral titanium-phosphonate material based on a tripodal peptide scaffold was used as a heterogeneous reaction medium for the enantioselective hydration (>99%) of styrene oxide [63].

5.2 Multifunctional materials

By combining chirality with other physical or chemical properties, multifunctional materials can be obtained. Although many chiral systems with additional functions have been reported, the direct influence of chirality on physical

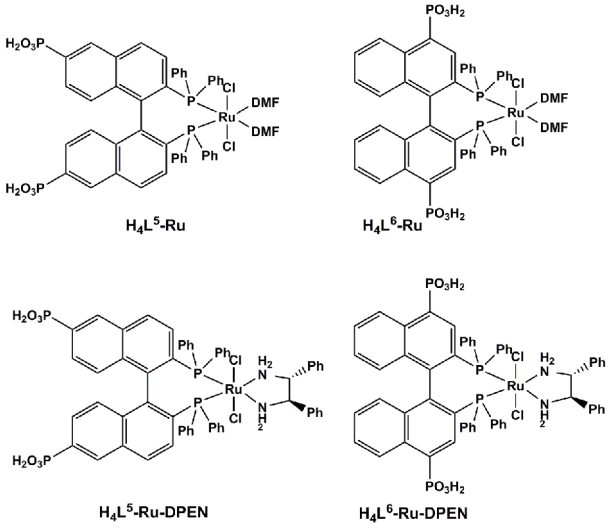

Scheme 5 Molecular structures of Ru complexes of binaphthalene-bisphosphonic acids.

properties such as magnetism and luminescence constitutes a relatively recent challenge [2]. For chiral metal phosphonates, there are still few examples showing coexistence of chirality and other functions. Studies on the coupling between chirality and other functions are extremely rare.

Chiral metal phosphonates are optically active, expressed as optical rotation or circular dichroism. Nonlinear optical properties were investigated in a few cases, and second-harmonic generation (SHG) effect was observed in several homochiral Zn/pemp compounds [49,50], (*R*)-,(*S*)-[Ln(pempH)$(NO_3)_2(H_2O)_2$] (Ln=Eu, Tb, Ho) [54] and the [Mn^{III}(5-Brsalcy)]/phosphonate compounds [59]. Characteristic luminescent properties were also observed in some Eu and Tb phosphonate compounds [45,54]. As expected, different coordination geometries of the lanthanide ions could affect the intensities of the emission peaks. For example, compounds (*R*)-[Er_4(pempH)$_{12}$]•7H_2O (*R*-**46**) and (*R*)-[Er_3(pempH)$_7$(pempH$_2$)$_2$]$(NO_3)_2$•2H_2O (*R*-**47**) contain seven- or eight-coordinated Er atoms, whereas (*R*)-[Er_2(pempH)$_4$$(NO_3)$Cl] (*R*-**48**) and (*R*)-[Er_2(pempH)$_4Cl_2$] (*R*-**49**) contain six-coordinated Er atoms [56]. Although all exhibit well-resolved multiline emission bands in the near-infrared region ranging from 1,450 to 1,630 nm with similar overall profiles, the strongest peak in *R*-**48** and *R*-**49** is centered at 1,540 nm (vs. 1,532 nm in *R*-**46** and *R*-**47**), and the peaks at ca. 1,490, 1,560, and 1,608 nm are largely reduced or even invisible. The different coordination geometries lead to different ligand-field effects which is responsible for the difference in the emission spectra.

Metal phosphonates can be promising proton conductors not only because of the presence of phosphonic acid groups to act as a proton source but also due to their high thermal and water stabilities compared to other types of coordination polymers [16]. Chiral metal phosphonate containing partially protonated phosphonate groups could be proton conductive multifunctional materials. For example, chiral compound Cs(HOOCCH(OH)PO_3H) (**7**) exhibits conductivity of 3.5 $\times10^{-5}$ S cm^{-1} at 24 °C despite the anhydrous nature [37]. Cd_2(D-pmpcH)$(H_2O)_2Cl_2$ (**26**) displays good water stability, moderate proton conductivity of 1.38×10^{-4} S cm^{-1} at 323 K and ~97% relative humidity, and a lower activation energy of 0.14 eV [48].

Some chiral metal phosphonates are porous and show adsorption properties. For example, the dehydrated samples of [Ln(H_2L^8)$_3$]•2H_2O [Ln=Tb (**17**), Dy (**18**), Eu (**19**), Gd (**20**)] show a selective sorption of N_2, H_2O and CH_3OH. over CH_3CH_2OH [45]. We found that chiral compounds [Fe(pemp)$(H_2O)_2$] (**33**) with nanotubular structures show highly selective adsorption capability towards NO gas due to the presence of open iron sites and narrow channel space [52].

Combination of chirality with magnetism is also very interesting [24], which can produce new multifunctional materials such as multiferroics [64] and bring new effects such as magnetochiral dichroism (MChD) effect [65] and chirality-induced spin selectivity (CISS) effect [66].

Considering the presence of strong spin-orbit coupling and the Kramers ground state in dysprosium complexes which are important for the development of high performance single molecule magnets (SMM), we studied the magnetic properties of the *R*-isomers of [Dy_3(pempH)$_7$(pempH$_2$)$_2$]$_2$$(NO_3)_4$•12$H_2O$ (**42**), [Dy_3(pempH)$_7$(pempH$_2$)$_2$]X_2•2H_2O [X=Cl (**43**), Br (**44**)] and [Dy_{11}(pempH$_2$)$_6$(pempH)$_{27}$]$(CF_3SO_3)_6$•22H_2O (**45**) [55]. A distinct SMM behavior with dual relaxation process is observed for compounds *R*-**43** and *R*-**44** at zero dc field with the effective energy barriers of 79.1 and 37.6 K for X=Cl, and 80.0 and 39.1 K for X=Br. For compounds *R*-**42** and *R*-**45**, slow magnetic relaxation is also observed but without the appearance of maxima down to 1.8 K. The results demonstrated that the magnetic behavior of the positively charged Dy^{III} chain compounds can be modulated by counter-anions.

Examples of chiral metal phosphonates showing long-range magnetic ordering are scarce. Compounds [Fe(pemp)$(H_2O)_2$] (**33**) display metamagnetism at low temperature [52]. The critical field (H_c) is 25 kOe at 2 K. Metamagnetism was also observed in enantiomeric compounds Co_2(μ_3-OH)(cyamp)(C_nH_{2n+1}COO) [*n*=1 (**52**), 7 (**53**)] which contain layers made up of Δ-type chains of corner-sharing triangles of Co_3(μ_3-OH) and O-P-O linkages [58]. The critical field decreases with the increasing interlayer distance from 8.18 kOe for *n*=1 to 7.01 kOe for *n*=7 at 1.8 K. Interestingly, enantioenriched compound Co_2(μ_3-OH)(4-cnapp)$(H_2O)_2$ (**33**) shows a three-dimensional framework structure in which the Δ-type chains of corner-sharing Co_3(μ_3-OH) triangles are cross-linked by the organic groups of the phosphonate ligands. Dominant antiferromagnetic interactions are again present between the Co^{II} centers. But in this case, the material is a soft magnet showing spontaneous magnetization at low temperature due to the presence of spin-canting effect. Slow magnetization relaxation is observed, attributed to the SCM-like behavior with spin-canted structure and/or domain wall movement. A least-squares fit based on the Arrhenius relationship $\tau(T)=\tau_0\exp(U_{eff}/k_BT)$, where τ_0 is the pre-exponential factor and U_{eff} is the effective energy barrier, leads to parameters $\tau_0=3.3\times10^{-9}$ s and U_{eff}/k_B= 59.6 K.

Another interesting examples are enantiopure compounds (*R*)-, (*S*)-Co_3(ppap)$_2$(4,4′-bpy)$_2$$(H_2O)_2$•4$H_2O$ (**21**) and (*R*)-, (*S*)-Co_3(ppap)$_2$(4,4′-bpy)$_2$$(H_2O)_2$•3$H_2O$ (**22**) and racemic compound *Rac*-Co_3(ppap)$_2$(4,4′-bpy)$_2$$(H_2O)_2$•4$H_2O$ [46]. Compounds **21** and **22** are catenation isomers showing 3D framework and layer structures, respectively. While compounds **21** and *Rac*-Co_3(ppap)$_2$(4,4′-bpy)$_2$$(H_2O)_2$•4$H_2O$ are isomers with the same chemical composition and identical framework structure (Figure 25(a, c)). Magnetic studies on the *S*-isomers and racemic species reveal that all three show

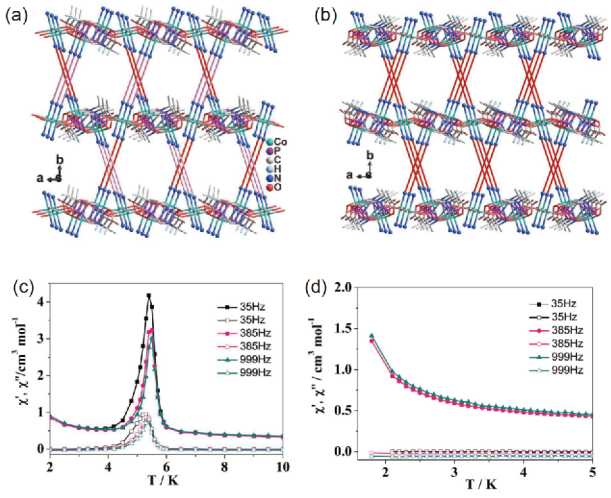

Figure 25 (a, c) Packing diagrams and (b, d) ac magnetic susceptibilities at zero external field for compounds (*S*)-**21** (a, b) and *Rac*-$Co_3(ppap)_2(4,4'\text{-bpy})_2(H_2O)_2\cdot 4H_2O$ (c, d), adapted with permission from Ref. [46], copyright by Wiley-VCH (2015) (color online).

paramagnetic properties down to 1.8 K. However, significant differences are found in their dehydrated forms. Long-range magnetic ordering occurs for the dehydrated samples of *S*-**21** (Figure 25(b)) and *S*-**22** due to spin-canting with the ordering temperature of 5.5 K and clear hysteresis loops below the ordering temperature. The canting angles are 1.0° and 5.0° for the two compounds, respectively. In contrast, the dehydrated racemic sample shows paramagnetism without ordering down to 1.8 K (Figure 25(d)), which can be explained by its structurally centrosymmetric nature. This work provides a rare example of chiral molecular systems that chirality can directly influence the magnetism.

6 Concluding remarks and outlook

This review summarizes the current status of chiral metal phosphonates including the syntheses, structures, morphology and properties. With regard to the syntheses, the enantioenriched or homochiral metal phosphonates can be obtained by using either achiral or chiral ligands. However, it is often a luck to achieve enantioenriched products through spontaneous symmetry breaking upon crystallization from achiral ligands. The underline mechanism is still far from being understood. A more efficient route towards chiral metal phosphonates is using chiral phosphonate ligands or co-ligands. So far most of homochiral metal phosphonates were synthesized using chiral phosphonate ligands. Those using other chiral co-ligands remain largely unexplored.

Studies on the physical and chemical properties of chiral metal phosphonates are still rather limited. Only in a few systems, the enantioselective catalytic and separation properties have been investigated. Coexistence of chirality and other functions such as NLO, luminescence, proton conductivity, sorption and magnetism have been explored in a few chiral metal phosphonates. But the influence of chirality on the other functions has been observed only in one case [46].

Great challenges remain in developing this field. First, how to design and synthesize chiral metal phosphonates with desirable structures and functions. Using enantiopure phosphonate ligands containing suitable organic groups is certainly a good solution. However, considering the difficulties in synthesizing enantiopure phosphonate ligands and the presence of large amount of achiral phosphonate ligands, the combination of achiral phosphonate ligand with chiral co-ligand could also be an economic and promising approach to synthesize new chiral metal phosphonates with particular structures and functions. Second, multifunctional chiral metal phosphonate systems need to be further explored. Though the coexistence of chirality and other functions in the same molecular composite is practically feasible, it is challenging to achieve coupling and modulation of multifunctions, especially the influence of chirality on other physical properties. Third, how to achieve chirality transcription and amplification from molecular level to helical structure in chiral metal phosphonate systems and understand the underline mechanisms. This phenomenon is common in nature, but hardly realized in synthetic systems. The exploration of chiral metal phosphonates with hierarchical helical morphologies is still in its infancy. Considering the importance of phosphorus chemistry in biological systems, the realization of chirality transcription from molecules to morphologies in chiral metal phosphonate systems would be significant for understanding bio-related self-assembly processes on the nano- to macro-scale.

Acknowledgements This work was supported by the National Natural Science Foundation of China (21731003, 91956102).

Conflict of interest The authors declare that they have no conflict of interest.

1 Wagnière GH. *On Chirality and the Universal Asymmetry*. Weinheim: Wiley-VCH, 2007
2 Pop F, Zigon N, Avarvari N. *Chem Rev*, 2019, 119: 8435–8478
3 Ma L, Abney C, Lin W. *Chem Soc Rev*, 2009, 38: 1248–1256
4 Shaw S, White JD. *Chem Rev*, 2019, 119: 9381–9426
5 Pan M, Wu K, Zhang JH, Su CY. *Coord Chem Rev*, 2019, 378: 333–349
6 Shang X, Song I, Jung GY, Choi W, Ohtsu H, Lee JH, Koo JY, Liu B, Ahn J, Kawano M, Kwak SK, Oh JH. *Nat Commun*, 2018, 9: 3933
7 Han Z, Wang K, Guo Y, Chen W, Zhang J, Zhang X, Siligardi G, Yang S, Zhou Z, Sun P, Shi W, Cheng P. *Nat Commun*, 2019, 10: 5117
8 Clearfield A. *Progress in Inorganic Chemistry*, *Vol 47*. New York: John Wiley & Sons, 1998. 371–510
9 Clearfield A, Demadis K. Eds. *Metal Phosphonate Chemistry: From Synthesis to Applications*. London: Royal Society of Chemistry, 2012
10 (a) Mao JG. *Coord Chem Rev*, 2007, 251:1493–1520; (b). Yang W, Parker TG, Sun ZM. *Coord Chem Rev*, 2015, 303: 86–109

11 Bao SS, Zheng LM. *Coord Chem Rev*, 2016, 319: 63–85
12 Shearan SJI, Stock N, Emmerling F, Demel J, Wright PA, Demadis KD, Vassaki M, Costantino F, Vivani R, Sallard S, Ruiz Salcedo I, Cabeza A, Taddei M. *Crystals*, 2019, 9: 270
13 Yücesan G, Zorlu Y, Stricker M, Beckmann J. *Coord Chem Rev*, 2018, 369: 105–122
14 Firmino ADG, Figueira F, Tomé JPC, Paz FAA, Rocha J. *Coord Chem Rev*, 2018, 355: 133–149
15 Bhanja P, Na J, Jing T, Lin J, Wakihara T, Bhaumik A, Yamauchi Y. *Chem Mater*, 2019, 31: 5343–5362
16 Bao SS, Shimizu GKH, Zheng LM. *Coord Chem Rev*, 2019, 378: 577–594
17 Fredoueil F, Evain M, Bujoli-Doeuff M, Bujoli B. *Eur J Inorg Chem*, 1999, 7: 1077–1079
18 Fredoueil F, Evain M, Massiot D, Bujoli-Doeuff M, Bujoli B. *J Mater Chem,* 2001, 11: 1106–1110
19 Evans OR, Ngo HL, Lin W. *J Am Chem Soc*, 2001, 123: 10395–10396
20 Evans OR, Manke DR, Lin W. *Chem Mater*, 2002, 14: 3866–3874
21 Ngo HL, Lin W. *J Am Chem Soc*, 2002, 124: 14298–14299
22 Huang J, Ding HM, Xu Y, Zeng D, Zhu H, Zang DM, Bao SS, Ma YQ, Zheng LM. *Nat Commun*, 2017, 8: 2131
23 Pérez-García L, Amabilino DB. *Chem Soc Rev*, 2007, 36: 941–967
24 Train C, Gruselle M, Verdaguer M. *Chem Soc Rev*, 2011, 40: 3297–3312
25 Morris RE, Bu X. *Nat Chem*, 2010, 2: 353–361
26 Li JT, Keene TD, Cao DK, Decurtins S, Zheng LM. *CrystEngComm*, 2009, 11: 1255–1260
27 Wang PF, Cao DK, Bao SS, Jin HJ, Li YZ, Wang TW, Zheng LM. *Dalton Trans*, 2011, 40: 1307–1312
28 Adelani PO, Albrecht-Schmitt TE. *Cryst Growth Des*, 2011, 11: 4676–4683
29 Yang XJ, Bao SS, Zheng T, Zheng LM. *Chem Commun*, 2012, 48: 6565–6567
30 Chen Z, Zhou Y, Weng L, Zhao D. *Cryst Growth Des*, 2008, 8: 4045–4053
31 Li JT, Cao DK, Liu B, Li YZ, Zheng LM. *Cryst Growth Des*, 2008, 8: 2950–2953
32 Jiao CQ, Zhao Z, Ma C, Sun ZG, Dong DP, Zhu YY, Li J. *Cryst Growth Des*, 2016, 16: 5624–5635
33 Liu B, Xu Y, Bao SS, Huang XD, Liu M, Zheng LM. *Inorg Chem*, 2016, 55: 9521–9523
34 Hou SZ, Cao DK, Li YZ, Zheng LM. *Inorg Chem*, 2008, 47: 10211–10213
35 Zheng T, Gao Y, Chen L, Liu Z, Diwu J, Chai Z, Albrecht-Schmitt TE, Wang S. *Dalton Trans*, 2015, 44: 18158–18166
36 Gao CY, Wang F, Tian HR, Li LJ, Zhang J, Sun ZM. *Inorg Chem*, 2016, 55: 537–539
37 Bazaga-García M, Papadaki M, Colodrero RMP, Olivera-Pastor P, Losilla ER, Nieto-Ortega B, Aranda MÁG, Choquesillo-Lazarte D, Cabeza A, Demadis KD. *Chem Mater*, 2015, 27: 424–435
38 Shiozawa T, Hossain MK, Ubukata T, Yokoyama Y. *Chem Commun*, 2010, 46: 4785–4787
39 Shi X, Zhu G, Qiu S, Huang K, Yu J, Xu R. *Angew Chem Int Ed*, 2004, 43: 6482–6485
40 Turner A, Jaffrès PA, MacLean EJ, Villemin D, McKee V, Hix GB. *Dalton Trans*, 2003, 7: 1314–1319
41 Sun ZG, Cui LY, Liu ZM, Dong DP, Meng L, Chen H, Zhang LC, Zhu ZM, You WS. *InOrg Chem Commun*, 2006, 9: 1121–1124
42 Yang BP, Mao JG. *J Mol Structure*, 2007, 830: 78–84
43 Yang BP, Mao JG, Sun YQ, Zhao HH, Clearfield A. *Eur J Inorg Chem*, 2003, 23: 4211–4217
44 Liu HY, Zhao B, Shi W, Zhang ZJ, Cheng P, Liao DZ, Yan SP. *Eur J Inorg Chem*, 2009, 18: 2599–2602
45 Yue Q, Yang J, Li GH, Li GD, Chen JS. *Inorg Chem*, 2006, 45: 4431–4439
46 Feng JS, Bao SS, Ren M, Cai ZS, Zheng LM. *Chem Eur J*, 2015, 21: 17336–17343
47 Liang X, Zhang F, Feng W, Zou X, Zhao C, Na H, Liu C, Sun F, Zhu G. *Chem Sci*, 2013, 4: 983–992
48 Liang X, Cai K, Zhang F, Liu J, Zhu G. *CrystEngComm*, 2017, 19: 6325–6332
49 Liu XG, Bao SS, Li YZ, Zheng LM. *Inorg Chem*, 2008, 47: 5525–5527
50 Liu XG, Huang J, Bao SS, Li YZ, Zheng LM. *Dalton Trans*, 2009, 9837
51 Liu XG, Bao SS, Huang J, Otsubo K, Feng JS, Ren M, Hu FC, Sun Z, Zheng LM, Wei S, Kitagawa H. *Chem Commun*, 2015, 51: 15141–15144
52 Jia JG, Feng JS, Huang XD, Bao SS, Zheng LM. *Chem Commun*, 2019, 55: 2825–2828
53 Liu M, Feng JS, Bao SS, Zheng LM. *Chem Eur J*, 2017, 23: 1086–1092
54 Liu XG, Zhou K, Dong J, Zhu CJ, Bao SS, Zheng LM. *Inorg Chem*, 2009, 48: 1901–1905
55 Xu Y, Yu YS, Huang XD, Bao SS, Ding HM, Ma YQ, Zheng LM. *Inorg Chem*, 2018, 57: 12143–12154
56 Xu Y, Bao SS, Huang XD, Zheng LM. *Cryst Growth Des*, 2018, 18: 4045–4053
57 An BH, Zhang RF, Li QL, Du XM, Ru J, Zhang SL, Ma CL. *J Organomet Chem*, 2019, 881: 51–57
58 Cai ZS, Bao SS, Ren M, Zheng LM. *Chem Eur J*, 2014, 20: 17137–17142
59 Wang TT, Bao SS, Huang J, Li YZ, Zheng LM. *Dalton Trans*, 2013, 42: 1842–1847
60 Hu A, Ngo HL, Lin W. *Angew Chem*, 2003, 115: 6182–6185
61 Hu A, Ngo HL, Lin W. *J Am Chem Soc*, 2003, 125: 11490–11491
62 Costantino U, Fringuelli F, Nocchetti M, Piermatti O. *Appl Catal A-General*, 2007, 326: 100–105
63 Milo A, Neumann R. *Adv Synth Catal*, 2010, 352: 2159–2165
64 Scarrozza M, Filippetti A, Fiorentini V. *Phys Rev Lett*, 2012, 109: 217202
65 Rikken GLJA, Raupach E. *Nature*, 1997, 390: 493–494
66 Göhler B, Hamelbeck V, Markus TZ, Kettner M, Hanne GF, Vager Z, Naaman R, Zacharias H. *Science*, 2011, 331: 894–897